haematologica
Journal of the Ferrata Storti Foundation

Longitudinal mechanisms of response, resistance and relapse to teclistamab in multiple myeloma: results from MajesTEC-1

by Deeksha Vishwamitra, Sheri Skerget, Diana Cortes-Selva, Tatiana Perova, Onsay Lau, Cuc Davis, Rengasamy Boominathan, Jaymala Patel, Koen Van den Berge, Yue Guo, Xin Miao, Tara Stephenson, Caroline Hodin, Clarissa Uhlar, Lixia Pei, Danielle Trancucci, Athena F. Zuppa, Katherine Chastain, Arnob Banerjee, Rachel Kobos, Nizar J. Bahlis, Niels W.C.J. van de Donk and Raluca I. Verona

Received: January 12, 2026.
Accepted: May 22, 2026.

Citation: Deeksha Vishwamitra, Sheri Skerget, Diana Cortes-Selva, Tatiana Perova, Onsay Lau, Cuc Davis, Rengasamy Boominathan, Jaymala Patel, Koen Van den Berge, Yue Guo, Xin Miao, Tara Stephenson, Caroline Hodin, Clarissa Uhlar, Lixia Pei, Danielle Trancucci, Athena F. Zuppa, Katherine Chastain, Arnob Banerjee, Rachel Kobos, Nizar J. Bahlis, Niels W.C.J. van de Donk and Raluca I. Verona. Longitudinal mechanisms of response, resistance and relapse to teclistamab in multiple myeloma: results from MajesTEC-1. Haematologica. 2026 June 11. doi: 10.3324/haematol.2026.300526 [Epub ahead of print]

Longitudinal mechanisms of response, resistance and relapse to teclistamab in multiple myeloma: results from MajesTEC-1

Deeksha Vishwamitra,[1] Sheri Skerget,[1] Diana Cortes-Selva,[1] Tatiana Perova,[1] Onsay Lau,[1] Cuc Davis,[1] Rengasamy Boominathan,[1] Jaymala Patel,[1] Koen Van den Berge,[2] Yue Guo,[1] Xin Miao,[1] Tara Stephenson,[1] Caroline Hodin,[2] Clarissa Uhlar,[1] Lixia Pei,[3] Danielle Trancucci,[3] Athena F Zuppa,[3] Katherine Chastain,[3] Arnob Banerjee,[1] Rachel Kobos,[3] Nizar J Bahlis,[4] Niels WCJ van de Donk,[5] and Raluca I Verona[1]

[1]Johnson & Johnson, Spring House, PA, USA.

[2]Johnson & Johnson, Beerse, Belgium.

[3]Johnson & Johnson, Raritan, NJ, USA.

[4]Arnie Charbonneau Cancer Institute, University of Calgary, Calgary, AB, Canada.

[5]Amsterdam University Medical Center, Vrije Universiteit Amsterdam, Amsterdam, The Netherlands.

Correspondence

Corresponding Author: Deeksha Vishwamitra

Address: 1400 McKean Road, Spring House, PA 19477

Email: dvishwam@its.jnj.com

Telephone: 619-614-4188

Running Title: *Mechanisms of Resistance/Relapse to Teclistamab*

Scientific category: Clinical Trials and Observations

ClinicalTrials.gov identifier: NCT03145181/NCT04557098

Data Sharing Statement

The data sharing policy of Johnson & Johnson is available at https://www.janssen.com/clinical-trials/transparency. As noted on this site, requests for access to the study data can be submitted through Yale Open Data Access (YODA) Project site at http://yoda.yale.edu.

Authorship contributions

DV, TS, CH, CU, LP, DT, AZ, KC, AB, RK, and RIV were responsible for the design of the study. DV, SS, DC-S, TP, OL, CD, RB, JP, YG, XM, and RIV collected the data. DV, SS, DC-S, TP, OL, CD, RB, KVdB, YG, XM, NJB, NWCJvdD, and RIV analyzed and interpreted the data. DV, SS, DC-S, TP, KVdB, NJB, NWCJvdD, and RIV participated in drafting the manuscript. All authors reviewed and approved the final version of the manuscript.

Funding

This study was funded by Johnson & Johnson.

Acknowledgments

We thank the patients who volunteered to participate in the study, their families and caregivers, the physicians and nurses who cared for the patients and supported this clinical trial, and staff members involved in data collection and analysis. The authors acknowledge Aniko Meijer and Jan Slabbaert for their valuable contributions to mass cytometry analyses and Sergi Hervás Fernandez for analysis support. Medical writing support was provided by Edwin C Thrower, PhD, CMPP, of Eloquent Scientific Solutions, and Holly Clarke, PhD, and Bethany Reinecke, PhD, CMPP, of Lumanity Communications, Inc., and funded by Johnson & Johnson.

Disclosure of Conflicts of Interest

NWCJvdD received research support from Janssen Pharmaceuticals, Amgen, Celgene, Novartis, Cellectis, and Bristol Myers Squibb; and served on advisory boards for Janssen Pharmaceuticals, Amgen, Celgene, Bristol Myers Squibb, Sanofi, Takeda, Roche, Novartis, Bayer, Adaptive, Kite Pharma, Merck, Pfizer, AbbVie, and Servier (all paid to institution). NJB consulted or served in an advisory role for Amgen and Celgene; and received honoraria from Amgen and Celgene. DV, SS, DC-S, TP, PL, CD, RB, JP, KVdB, YG, XM, TS, CH, CU, LP, DT, AZ, KC, AB, RK, and RIV were employed by Johnson & Johnson at the time the study was conducted and may have stock or stock options in Johnson & Johnson.

Abstract <<250 / 250>>

Previous studies have shown that response to teclistamab, the first approved B-cell maturation antigen (BCMA)–directed bispecific antibody for the treatment of triple-class–exposed relapsed/refractory multiple myeloma, was associated with baseline immune fitness, while nonresponders had profiles suggestive of immune suppression and T-cell dysfunction. Here, we correlated longitudinal peripheral and tumor microenvironment immune profiles and BCMA antigen expression with teclistamab clinical response, resistance, and relapse in MajesTEC-1 (ClinicalTrials.gov Identifiers: NCT03145181/NCT04557098). Bone marrow and peripheral blood samples were collected at baseline, on treatment, and at disease progression. Teclistamab responders exhibited greater T-cell margination, recovery, and increased T-cell activation compared with nonresponders in the periphery. After teclistamab treatment, nonresponders generally exhibited trends for elevated and sustained expression of checkpoint markers on CD4+ and CD8+ T cells, suggestive of persistent T cell activation, and higher, sustained proportions of immunosuppressive regulatory T cells longitudinally, which could contribute to resistance. At relapse, higher proportions of peripheral and bone marrow CD4+ and CD8+ T cells expressing markers associated with T-cell dysfunction and impairment (eg, CD39 and CD57) and higher proportions of regulatory T cells were observed compared with baseline. Finally, a reduction in BCMA receptor density was observed on bone marrow tumor plasma cells at relapse. Our data highlight the importance of understanding mechanisms of response, resistance, and relapse to teclistamab to optimize T-cell and bispecific antibody activity, advance dosing and sequencing strategies, and inform further evaluation of teclistamab combinations with other anti–myeloma agents and use in earlier lines of treatment to improve patient outcomes.

Introduction

Treatment strategies for multiple myeloma (MM) have greatly improved in recent years, with the current standard of care including immunomodulatory drugs (IMiDs), proteasome inhibitors, and anti-CD38 monoclonal antibodies.[1-3] However, many patients become refractory to these initial therapies and experience disease relapse.[4-6] An unmet need remains for additional effective therapies that can be well tolerated in patients who develop relapsed/refractory MM (RRMM).

Teclistamab is the first approved B-cell maturation antigen (BCMA) × CD3 bispecific antibody (BsAb) for the treatment of triple-class–exposed RRMM,[7,8] with weight-based dosing and more than 23,000 patients treated worldwide.[9] In the phase 1/2 MajesTEC-1 study (ClinicalTrials.gov Identifiers: NCT03145181/NCT04557098), deep and durable responses were attained with teclistamab monotherapy in 165 heavily pretreated patients with RRMM.[10]

Emerging translational research has indicated that immune cell composition contributes to immunotherapeutic responses[11]; therefore, the efficacy of teclistamab, as a T cell redirection therapy, may be influenced by immune fitness.[12] In a recent report, we demonstrated that immune profiles and tumor characteristics at baseline correlated with clinical response in patients with RRMM from the MajesTEC-1 study.[13] Teclistamab-responsive patients exhibited higher baseline total T cell counts and expression of cytotoxic factors (eg, granzyme B and perforin) in the periphery and bone marrow, with reduced expression of markers associated with T cell dysfunction.[13] In addition, improved progression-free survival was associated with a favorable baseline T cell signature, such as lower proportions of regulatory T cells and lower expression of inhibitory receptors on T cells.

In the current study, we assessed the longitudinal peripheral and tumor microenvironment immune profiles, as well as tumor antigen expression, and their association with response,

resistance, and relapse in patients treated with teclistamab in MajesTEC-1. This is the first publication to present analyses on potential resistance mechanisms of teclistamab from a large, comprehensive, pivotal dataset. The findings build on the emerging data in the field and advance our understanding of mechanisms of response, resistance, and relapse to teclistamab. Such insights may inform strategies for dose optimization, treatment sequencing, and the development of more effective multi-agent approaches. This work provides the foundation for ongoing studies of multi-target approaches, including combinations of teclistamab with other anti-MM agents (ie, daratumumab, talquetamab, or IMiDs).[14,15] Thus, the mechanistic insights gained here may ultimately help improve the depth and duration of response for patients.

Methods

Study design and patient population

Full details of the study design of MajesTEC-1 (NCT03145181/NCT04557098) have been previously published,[16,17] and are summarized in the **Supplemental Appendix**. Briefly, 165 patients with RRMM who had received ≥3 prior lines of therapy, received subcutaneous teclistamab 1.5 mg/kg weekly, following step-up doses (0.06 mg/kg and 0.3 mg/kg). Teclistamab responders were defined as patients who achieved a best clinical response of partial response or better (≥PR) per International Myeloma Working Group (IMWG) criteria,[18,19] as assessed by an independent review committee; patients who did not achieve this, or had a non-evaluable response, were considered nonresponders. These data were analyzed at the clinical cutoff date of August 22, 2023.

MajesTEC-1 was conducted in accordance with the principles of the Declaration of Helsinki and Good Clinical Practice guidelines of the International Council for Harmonisation. Study protocol and amendments were approved by each site's Institutional Review Board. All patients provided informed written consent.

Biological correlatives and CyTOF analyses

Sample collection is summarized in **Supplementary Figure 1**. Exploratory endpoints included assessment of soluble BCMA (sBCMA) using an electrochemiluminescence ligand-binding assay using the Meso Scale Discovery (MSD) platform and characterization of T cell numbers and subsets, activation markers and co-inhibitory receptor expression in peripheral blood and tumor samples, and membrane-bound BCMA expression on tumor plasma cells using flow cytometry. The Wilcoxon rank-sum test was performed to identify relevant immune correlatives that differed between responders and nonresponders or differed between time points. For each patient, fold change from baseline for a particular biomarker was calculated as the value at the time point of interest versus the baseline value. Maximum fold change (max FC) was calculated by determining the highest FC from available measurements between specified timepoints for each patient.

Peripheral blood and bone marrow samples from 25 and 23 patients respectively were collected and processed using cytometry by time-of-flight (CyTOF) mass cytometry. Two antibody panels (40 markers for blood, 44 for bone marrow, **Supplemental Table 1 and 2**) were utilized. Samples were analyzed on a Helios mass cytometer (Standard BioTools) and data were normalized using CyTOF software (Standard BioTools). Briefly, quality control for batch effects at the sample and cluster level were performed using hilbertSimilarity[20] and Earth Mover's Distance,[21] respectively. Marker staining consistency across batches was evaluated using marker enrichment modeling.[22] Batch effect correction was applied using cyCombine.[23] Cell clustering and annotation were done using FlowSOM,[24] and polyfunctionality analysis of T cell subsets was conducted using FreeViz projections,[25] with the differences modelled using linear mixed model analysis.

The **Supplemental Appendix** provides additional details regarding the methods and statistical analyses.

Results

Greater T cell reduction and recovery is observed in the peripheral blood in responders following teclistamab

Consistent with T cell margination, there was an initial reduction in absolute counts of CD4+ and CD8+ T cells in the periphery within 24 hours following the administration of the first step-up dose of teclistamab (**Figure 1A-F**). Patients who responded to teclistamab demonstrated a greater and more rapid reduction in CD4+ and CD8+ T cells compared with nonresponders (CD4+ step-up dose 1 predose [SUD1_PRE] vs after 24 hours [SUD1_24H]: responders, –85% [*P* <0.001]; nonresponders, –36%; CD8+ SUD1_PRE vs SUD1_24H: responders, –80% [*P* <0.001]; nonresponders, –65%; **Figure 1A-B**, **red outlines**). The max FC reduction during the margination period was significantly different between responders and nonresponders for CD4+ and CD8+ T cells (median max FC SUD1_PRE vs SUD1_24H, responders vs nonresponders: CD4+: 0.35 vs 0.92, *P*<0.05; CD8+: 0.19 vs 0.68, *P*<0.05; **Figure 1C-D**). This was followed by greater T cell recovery after the first full treatment dose of teclistamab on Cycle (C) 1 Day (D) 1 in responders compared with nonresponders, with increased absolute counts of CD4+ and CD8+ T cells persisting through C3D1, indicating proliferation of T cells in the periphery (CD4+ SUD1_24H vs C3D1: responders, +604% [*P* <0.001]; nonresponders, –59%; CD8+ SUD1_24H vs C3D1: responders, +322% [*P* <0.001]; nonresponders, –14%; **Figure 1A-B**, **blue outlines**). The max FC increase during recovery was significantly different between responders and nonresponders for CD8+ T cells (median max FC SUD1_24H to C3D1, responders vs nonresponders: CD8+: 0.90 vs 0.57; *P*<0.05; **Figure 1E-F**). Of note, both median CD4+ and CD8+ T cell counts in teclistamab responders recovered to near baseline levels by C3D1, whereas numbers remained low in nonresponders (median × 10^6/L, SUD1_PRE vs C3D1;

CD4+: responders, 175 vs 190; nonresponders, 168 vs 44; CD8+: responders, 180 vs 150; nonresponders, 214 vs 64).

Greater and earlier T cell activation in the peripheral blood observed in responders in early cycles

Given the initial changes in T cell numbers, we next evaluated the longitudinal profiles of T cell activation, namely the induction of CD38 on CD4+ and CD8+ T cells, in early cycles between responders and nonresponders after teclistamab treatment. The peak T cell activation period for responders was observed early during C1, as indicated by a transient increase in expression of CD38 on CD8+ T cells at C1D1 (**Figure 2A**). In contrast, nonresponders displayed a delayed T cell activation profile, with peak T cell activation occurring at C2D1 (**Figure 2A**). Additionally, patients who responded to teclistamab exhibited significantly higher max FC induction of CD38 expression on CD8+ T cells in the first cycle than nonresponding patients (max FC responders: 9 vs max FC nonresponders: 6; P <0.05; **Figure 2B**), which may be indicative of greater T cell activation of cytotoxic T cells in responding patients. A comparable T cell activation profile was seen in induction of CD38 expression on CD4+ T cells (**Supplemental Figure 2A-B**). In contrast to CD38 induction, other activation markers, CD25 and HLA-DR, did not show significant differential activation profiles between responders and nonresponders (**Supplemental Figure 2C-J**).

Continued elevated expression of coinhibitory checkpoint markers and increased proportion of regulatory T cells observed in the peripheral blood in nonresponders

Since persistent activation of T cells and upregulation of coinhibitory receptors and checkpoints may be associated with an impaired T cell phenotype and resistance,[26] we examined the longitudinal expression patterns of LAG-3, TIM-3, PD-1, PD-1/LAG-3, and PD-1/TIM-3 on CD4+ and CD8+ T cells in the periphery after the peak T cell activation period (ie, >C2D1). For CD8+ T cells, responders generally exhibited a trend in decreased or lower proportions of coinhibitory

checkpoint markers from C2D1 to C3D1 compared to nonresponders, including LAG-3 (responders vs nonresponders: –1% vs +66%), TIM-3 (–54% vs +21%), PD-1/TIM-3 (–24% vs +29%), and PD-1/LAG-3–expressing T cells (+9% vs +148%), with an exception only seen with PD-1 (+21% vs +13%; **Figure 3A-E**). Similar trends were observed for CD4+ T cells (**Supplemental Figure 3A-E**). At C3D1, there were significantly higher (P<0.05) proportions of coinhibitory checkpoint markers for nonresponders than responders, including LAG-3, PD-1, PD-1/TIM-3, and PD-1/LAG-3 on both CD8+ and CD4+ T cells and TIM-3 on CD4+ T cells. (**Figure 3A-E and Supplemental Figure 3A-E).** Together, this may be suggestive of persistent T cell activation in nonresponders.

To further elucidate the contribution of other T cell subsets to a potentially dysfunctional phenotype in nonresponders to teclistamab, we analyzed the proportion of immunosuppressive regulatory T cells and CD38-expressing Tregs longitudinally. Significantly higher proportions of Tregs, including those expressing CD38, were present in the periphery in nonresponders compared with responders at baseline (P<0.05), and this was sustained over time, with significantly higher CD38+ Tregs at C3D1 in nonresponders than responders (P<0.05; **Figure 4A-B**). These findings further support a more immunosuppressive and impaired peripheral immune profile in nonresponding patients.

Immune changes in the bone marrow are comparable to peripheral immune profiles post teclistamab treatment

In addition to immune profiling in the periphery, we assessed changes in key immune subsets in the bone marrow to identify signatures associated with resistance stemming from the bone marrow microenvironment (**Figure 5A-G**). Compared with baseline, T cell infiltration was observed in responders at C3D1, as indicated by a modest increase in proportions of CD3+ T cells (baseline vs C3D1: +3% [P <0.001]), while nonresponders displayed lower levels of CD3+

T cells (-6%; **Figure 5A)**. Furthermore, consistent with the peripheral immune profiles, nonresponders exhibited a trend in increased proportions of coinhibitory receptors on CD4+ and CD8+ T cells at C3D1 compared with baseline, including higher PD-1 (baseline vs C3D1: CD4+, +69% [*P* <0.05]; CD8+, +13%), TIM-3 (baseline vs C3D1: CD4+, +7%; CD8+, +232% [*P*<0.01]), and PD-1/TIM-3 expression (CD4+, +308% [*P* <0.01]; CD8+, +677% [*P* <0.001]). Responders also exhibited increased proportions of coinhibitory receptors, but the magnitude of the increase was generally smaller than for nonresponders: PD-1 (CD4+, +51% [*P* <0.01]; CD8+, +12%), TIM-3 (baseline vs C3D1: CD4+, +88% [P<0.001]; CD8+, +184% [*P*<0.001]), and PD-1/TIM-3 (CD4+, +111% [*P* <0.001]; CD8+, +250% [*P* <0.001]). In agreement with the peripheral immune profiles, these findings potentially indicate persistent T cell activation in the bone marrow of nonresponding patients (**Figure 5B-G**).

A progression to impaired T cell phenotype observed in patients at relapse in the periphery and the bone marrow

Along with identifying resistance mechanisms in nonresponders, we sought to assess immune changes in responders who eventually relapsed to teclistamab. We first performed supervised CyTOF analysis on whole blood and bone marrow samples collected at baseline and at relapse using a manual gating strategy. In the periphery, we observed trends for lower frequencies of naïve T cells and higher frequencies of differentiated effector memory CD4+ and CD8+ subsets at relapse versus baseline (**Supplemental Figure 4A-B**). Furthermore, we observed significantly higher proportions of dysfunctional T cells at relapse, as indicated by increased proportions of CD4+ and CD8+ T cell expressing coinhibitory checkpoint markers, including PD-1, LAG-3, TIGIT, increased proportions of markers associated with T cell impairment and senescence, including CD39+, CD57+, and granzyme B, and reduced proportions of the costimulatory molecule CD28+ on CD8+ T cells, suggesting that a dysfunctional T cell phenotype in the periphery may contribute to relapse (**Supplemental Figure 4A-B**). In a

supervised CyTOF analysis of bone marrow samples, we observed upregulation of PD-1 and TIGIT on CD25hiCD127dim Tregs (**Supplemental Figure 4C-D**). Upregulation of these markers is thought to increase the immunosuppressive potential of Tregs, which may contribute to a dysfunctional T cell phenotype in the tumor microenvironment at relapse.[27]

We next performed polyfunctionality analyses of the CyTOF data. We used the FreeViz algorithm to identify differential marker expression and to further characterize the T cell phenotypes in the peripheral blood and the bone marrow at baseline and at relapse (**Figures 6 and 7 and Supplemental Table 1 and 2**). In the periphery, CD8+ T cell subsets were significantly enriched for the expression of PD-1, CD57, CD38, CD39, and CD45RO with markedly reduced expression of human leukocyte antigen-DR (HLA-DR), and CD45RA at relapse compared with baseline, which is indicative of an impaired phenotype (**Figure 6A**). In addition, we observed a significant enrichment for CD4+ T cells expressing PD-1, CD38, granzyme B, and killer cell lectin-like receptor G1 (KLRG1) and a depletion of CD4+ T cells expressing CD28, CD127, and CD27 (**Figure 6B**). In the bone marrow, polyfunctionality assessment revealed an enrichment for CD4+ and CD8+ T cell subsets expressing TOX, KLRG1, and PD-1 at relapse compared with baseline, suggesting a shift towards a state of immune dysfunction and senescence in the T cell compartment within the tumor microenvironment that may contribute to the mechanism of relapse in patients who received teclistamab (**Figure 7A-B**).

Flow cytometry analyses align and further support CyTOF findings, with an observed trend in the increase of CD38, PD-1, TIM-3, and PD-1/TIM-3 expression on CD4+ and CD8+ T cells in the periphery and bone marrow at the time of disease progression compared with baseline, similarly suggesting that a dysfunctional T cell phenotype contributes to relapse after

teclistamab treatment (**Supplemental Figures 5A-J and 6A-K**). In comparison, nonresponders exhibit an even more dysfunctional T cell phenotype compared to patients who responded and then relapsed, including greater reduction of absolute counts of CD8+ and CD4+ T cells and increased CD38, PD-1, TIM-3, and PD-1/TIM-3 expression on CD4+ and CD8+ T cells in the periphery (**Supplemental Figure 7A-K**).

Reduction in plasma cell BCMA receptor density observed at relapse versus baseline

In addition to immune signatures that may contribute to relapse after teclistamab treatment, we also assessed the impact of other factors, such as sBCMA levels, proportions of BCMA+ plasma cells, and BCMA receptor density in patients who relapsed relative to baseline and who also had evaluable samples for this analysis (**Supplemental Figure 8A-H**). Overall, compared with baseline, no significant change in the proportion of BCMA+ plasma cells was observed (**Supplemental Figure 8B** and **D**). However, a significant reduction in sBCMA and BCMA receptor density was noted at the time of relapse relative to baseline (**Supplemental Figure 8A** and **C**). Within-patient reductions in BCMA receptor density from baseline to relapse were observed for patients that responded and then progressed (**Supplemental Figure 8E**). Although data is limited, there does not appear to be a correlation between the length of response (<6 months or ≥6 months) and the reduction in sBCMA or receptor density (**Supplemental Figure 8F, G,** and **H**). Given the small sample sizes, additional analyses are needed; however, this reduction in BCMA receptor density may represent a selection of residual cells with lower BCMA levels, while tumor cells with higher BCMA expression have been eliminated.

Discussion

Building on existing literature,[11,12] we previously showed that baseline immune fitness and T cell function were important in achieving a clinical response and a longer progression-free survival

with teclistamab, while baseline T cell dysfunction and immune suppression were associated with nonresponse.[13] The current analysis of longitudinal correlatives expands on previous findings by showing the importance of improved T cell activity over time in achieving and maintaining a response to teclistamab while identifying potential mechanisms of resistance and relapse after teclistamab treatment. This work provides the foundation for ongoing studies of multi-target approaches, including combinations of teclistamab with other anti-MM agents (ie, daratumumab, talquetamab, or IMiDs).[14,15,28]

Differential immune profiles were observed longitudinally, with greater and more rapid T cell margination and recovery and earlier T cell activation in responders compared with nonresponders in the periphery. While the contribution of T cell margination to T cell engager response remains to be fully elucidated, increased T cell margination likely results from T cell activation and cytokine release, which cause the T cells to adhere to the endothelium and migrate to the tumor site. T cell margination has been shown to be associated with superior treatment responses,[29,30] thus these findings support T cell margination as a potential predictive marker of clinical outcomes.

We also observed greater recovery of both CD4+ and CD8+ T cells in the periphery by the first full treatment dose of teclistamab in responders, which was not evident in nonresponders, indicative of the potent proliferative capacity in responders possibly resulting from the decreased tumor burden after treatment, which may lead to an expansion of T cells that have robust cytotoxic activity and are able to respond to a strong immune stimulus.[13] In addition, increased proportions of CD3+ T cells were also observed in the bone marrow in responders at C3D1 compared with baseline, which may be suggestive of T cell infiltration. Expansion of phenotypically cytotoxic T cells in particular has been hypothesized to be relevant to the antitumor response.[12,31] Ongoing clinical trials are investigating teclistamab in combination with

immunomodulatory anti-myeloma agents, such as daratumumab and IMiDs, which may potentiate its effect by enhancing T-cell activity.[31] Responders exhibited greater max FC induction of CD38 on CD4+ and CD8+ T cells in the first 2 cycles compared with nonresponders, indicative of greater T cell activation.[32,33] Furthermore, peak T cell activation as assessed by CD38 occurred earlier in responders by the first full treatment dose on C1D1 of teclistamab, while nonresponders displayed a delayed T cell profile, with peak induction occurring by C2D1. These observations further suggest stronger initial T cell stimulation with optimal timing that may contribute to a more effective immune response in early cycles, thus contributing to an early response in responding patients.

In contrast to CD38 induction on CD8+ and CD4+ T cells, other activation markers, CD25 and HLA-DR, did not show significant differential activation profiles between responders and nonresponders, consistent with what has been demonstrated preclinically.[26] Considering HLA-DR and CD25 are markers in later activation states,[34,35] these results may potentially continue to support a more specific, perhaps early, T cell activation state following teclistamab treatment, particularly in responders. In addition, this pattern may differ from typical overactivation (high CD38+HLA-DR+), which is often associated with T cell dysfunction in various disease states.[36] The notable increase in CD38 in responders following teclistamab administration may also be particularly relevant in teclistamab-daratumumab combination therapy where the daratumumab targets and suppresses CD38+ T cells.[15]

Persistent stimulation of T cells leads to an impaired T cell phenotype, a state of T cell dysfunction often indicated by the upregulation of coinhibitory expression and markers of T cell impairment, immunosuppression, and senescence.[37] In our current analyses, we observed that nonresponders exhibited persistent T cell activation and sustained, higher levels of coinhibitory

checkpoint marker expression (PD-1, TIM-3, and LAG-3) in the blood and bone marrow compared with responders. The expression of inhibitory receptors, such as PD-1 and LAG-3, characterize continued T cell activation potentially leading to impaired T cell function. PD-1 signaling has been shown to reduce T cell receptor–induced proliferation, while LAG-3 signaling diminishes cytokine production and target cell killing, resulting in lower antitumor activity. Consequently, impaired T cells may hinder the efficacy of therapy, as shown here and in other studies.[12,26,39] Furthermore, in the current study, elevated proportions of peripheral immunosuppressive Tregs, and higher CD38-expression, were also observed in nonresponders. Previous findings support a high proportion of absolute Tregs dampening the proliferative capacity of T cells, impairing the ability of T cells to exert antitumor activity, and diminishing treatment outcomes.[40] Prior research also supports the heightened presence of CD38-expressing Tregs in patients with multiple myeloma and leukemia versus healthy donors,[41,42] with higher counts associated with impaired response to treatment.[26] A greater proportion of T cells expressing co-inhibitory markers may be expected in view of disease activity and increased disease burden, however, a lack of longitudinal tumor burden data limited the confirmation of definite correlation. It is important to note that, as assessed in our prior analysis, several of these coinhibitory biomarkers of interest were associated with clinical response groups independent of disease burden, such as expression of PD-1 and TIM-3, supporting their mechanistic role in the ability to respond to teclistamab treatment.[13] This evidence suggests that longitudinally, sustained expression of coinhibitory receptors on T cells may be an independent correlative in nonresponders. Collectively, the elevation of coinhibitory checkpoint marker expression and Tregs likely led to the hindrance of effective immune response and suppression of T cell function, characterizing a mechanism of resistance to teclistamab treatment present in nonresponders.

Although patients in MajesTEC-1 achieved a high overall response rate, some patients eventually experienced disease progression that prompted us to further evaluate mechanisms of relapse. Supervised analyses in the blood and bone marrow using CyTOF demonstrated findings such as increased proportions of effector memory, higher expression of inhibitory receptors (PD-1, LAG-3, and TIM-3), CD38, and granzyme B, as well as lower expression of CD28 on T cells in patients who relapsed. Previous evidence supports a lack of CD28 expression as a definitive marker of severe T cell impairment, with terminally differentiated and senescent features associated with dysfunction (ie, reduced interferon-γ production by CD4+ and CD8+ cells) and reduced degranulation capacity.[43] Supervised CyTOF analysis in the bone marrow also showed an upregulation of PD-1 and TIGIT on CD25hiCD127dim Tregs. TIGIT expression has been shown to be significantly higher in T cells of early relapse patients with RRMM, suggesting that T cell impairment driven by high TIGIT expression may underlie therapy relapse. Furthermore, TIGIT+ effector cells have been shown to display limited cytokine responses to antigen-specific stimulation and thus poor MM killing capability.

Unsupervised polyfunctionality analysis of CyTOF data in the blood and bone marrow further supported these findings. The bone marrow showed a shift towards immune dysfunction and senescence at relapse, with increased expression of TOX, KLRG1, and PD-1 on CD4+ and CD8+ T cells. In the periphery, CD8+ T cell subsets demonstrated an increased expression of PD-1, CD57, CD38, CD39, and CD45RO, and decreased HLA-DR and CD45RA expression, while CD4+ T cells exhibited higher levels of PD-1, CD38, granzyme B, and KLRG1, alongside reduced expression of CD28, CD127, and CD27, all of which further indicate an impaired phenotype at relapse compared with baseline. Flow cytometry data further corroborated these CyTOF findings, with an observed trend in the increase of CD38, PD-1, and PD-1/TIM-3 expression on CD4+ and CD8+ T cells in the periphery and bone marrow at the time of disease progression. Data suggest that relapsed patients exhibit a similar, but less pronounced,

dysfunctional T cell phenotype versus nonresponders, suggesting that patients who initially responded to teclistamab may exhibit a more favorable phenotype at relapse compared to patients who exhibited primary resistance, informing subsequent treatment strategies. In totality, our findings indicate the development of a dysfunctional immune phenotype with enhanced immunosuppressive activity, which may have contributed as a mechanism of relapse after teclistamab treatment.

Previous preclinical studies of various subsets of patients have shown that increased expression of dysfunction markers (PD-1, TIGIT, and TIM-3) and Tregs are associated with impaired MM cell killing and reduced antitumor efficacy in response to BsAb therapies, such as teclistamab and talquetamab.[26,39] Additionally, the presence of dysfunctional T cell clones predicts response failure to BCMA-targeting bispecific T cell engagers in patients with MM.[12] In light of all available evidence from this robust MajesTEC-1 dataset, our current findings further support the notion that persistent peripheral and bone marrow T cell activation and an immunosuppressive bone marrow microenvironment likely contributes to T cell dysfunction and teclistamab resistance and relapse in patients with MM. These results support combining BsAbs with immunomodulatory agents to achieve synergistic anti-myeloma effects, an approach currently under investigation in ongoing clinical trials.[31] For example, the observed increase in CD38+ Tregs longitudinally and at relapse support the inclusion of daratumumab given its capacity to deplete these immunosuppressive cells.

Previously, we demonstrated that baseline tumor BCMA expression did not correlate with clinical response, while baseline sBCMA levels did correlate with disease burden and clinical response, with responders showing significantly lower baseline sBCMA levels than nonresponders.[13,46] Additionally, in a recent analysis of the impact of the T cell landscape on response to BsAbs in RRMM, antigen loss of BCMA or major histocompatibility complex class I

surface expression on malignant plasma cells was observed in some clinical nonresponders (those with stable disease, minimal response, or progressive disease) at relapse.[12] In our current analysis, no significant change in the proportions of BCMA+ plasma cells were seen; however, sBCMA was significantly reduced at the time of disease progression suggesting that increasing sBCMA levels may not be a contributor to relapse. The reduction in sBCMA observed at relapse is likely due to reduced tumor burden from initial response to therapy. We also observed a significant reduction in BCMA receptor density in the bone marrow at the time of relapse and within-patient reductions from baseline to relapse were observed for patients that responded and then progressed. This reduction in BCMA receptor density may represent a selection of residual cells with lower BCMA levels, while tumor cells with higher BCMA expression have been eliminated, however further mechanisms of antigen loss cannot be excluded. Emerging data from a limited number of patients has shown that antigen loss or abrogation of anti-BCMA T cell engager binding may be driven by mutational events in BCMA in ≥40% of patients.[47] Further evaluations of samples assessing molecular alterations in this larger cohort of patients are ongoing and likely to provide additional insight on the nature of antigen escape in these relapsed patients treated with teclistamab.[12,47] Future studies will also evaluate whether dual antigen targeting, such as with combinations of teclistamab with talquetamab or daratumumab, can help overcome the antigen loss mechanisms observed with single-antigen approaches.[14,15,28]

While these results provide crucial insight into the association between immune profiles and response, resistance and relapse to teclistamab, several limitations are to be noted. Firstly, the sample size of nonresponders, at times, was relatively small compared with responders. These reduced numbers may have been due, in part, to non-responders coming off (ie, discontinuing) study treatment early following confirmed disease progression (per IMWG criteria), as outlined per-protocol. Furthermore, the low number of nonresponding patients inherently supports the

efficacy of teclistamab as a treatment option in this patient population. Secondly, although our CyTOF and flow results regarding peripheral T cell responses were highly correlated, functional testing of peripheral T cells was not performed as part of this study; therefore, future testing may be required to confirm our findings regarding effective T cell responses in responding patients. Thirdly, longitudinal tumor burden data was not measured as part of this study, preventing definitive assessment of the correlation between tumor burden and T cell changes, such as coinhibitory receptor expression longitudinally and at relapse.

In conclusion, our findings derived from the pivotal MajesTEC-1 study dataset, emphasize the importance of understanding the mechanisms of response, resistance, and relapse to teclistamab in order to optimize T cell and bispecific antibody activity. Teclistamab responders showed greater T-cell activation followed by recovery, whereas nonresponders trended towards sustained expression of checkpoint markers and regulatory T cells over time, suggesting persistent T cell activation, which may indicate T-cell dysfunction. Furthermore, at relapse, dysfunctional T cells and regulatory T cells were frequent, along with reduced BCMA receptor density on bone marrow tumor cells. Our findings build upon those of smaller subgroup studies, collectively contributing to the body of knowledge, and informing further evaluation of dosing strategies and combination therapy with other anti-MM agents, such as daratumumab, talquetamab, checkpoint inhibitors, or IMiDs, ultimately aiming to enhance patient outcomes. The data presented here will provide a foundation for analyses of dual antigen targeting that are currently under investigation. Gaining a better understanding of patients' immune profiles over time will be crucial in understanding potential mechanisms of resistance and relapse and for informing the optimization of new immunotherapy combinations to ensure utilization in the most clinically beneficial manner.

References

1. Mikhael J, Ismaila N, Cheung MC, et al. Treatment of multiple myeloma: ASCO and CCO Joint Clinical Practice Guideline. J Clin Oncol. 2019;37(14):1228-1263.

2. Moreau P, Richardson PG, Cavo M, et al. Proteasome inhibitors in multiple myeloma: 10 years later. Blood. 2012;120(5):947-959.

3. van de Donk N, Richardson PG, Malavasi F. CD38 antibodies in multiple myeloma: back to the future. Blood. 2018;131(1):13-29.

4. Kumar SK, Rajkumar SV, Dispenzieri A, et al. Improved survival in multiple myeloma and the impact of novel therapies. Blood. 2008;111(5):2516-2520.

5. Laubach J, Garderet L, Mahindra A, et al. Management of relapsed multiple myeloma: recommendations of the International Myeloma Working Group. Leukemia. 2016;30(5):1005-1017.

6. Mateos MV, Weisel K, De Stefano V, et al. LocoMMotion: a prospective, non-interventional, multinational study of real-life current standards of care in patients with relapsed and/or refractory multiple myeloma. Leukemia. 2022;36(5):1371-1376.

7. European Medicines Agency. EPAR summary of product characteristics. TECVAYLI [teclistamab]. Available at https://www.ema.europa.eu/en/documents/product-information/tecvayli-epar-product-information_en.pdf. Accessed May 18, 2026.

8. TECVAYLI® (teclistamab-cqyv) injection, for subcutaneous use [package insert]. Horsham, PA: Janssen Biotech, Inc.; 2026. Available at https://www.jnjlabels.com/package-insert/product-monograph/prescribing-information/TECVAYLI-pi.pdf. Accessed May 18, 2026.

9. Johnson & Johnson. Johnson & Johnson announces U.S. FDA approval of TECVAYLI® plus DARZALEX FASPRO® for relapsed/refractory multiple myeloma, offering a potential new standard of care as early as second line. Available at https://www.jnj.com/media-center/press-releases/johnson-johnson-announces-u-s-fda-approval-of-tecvayli-plus-darzalex-faspro-for-

relapsed-refractory-multiple-myeloma-offering-a-potential-new-standard-of-care-as-early-as-second-line. Accessed March 11, 2026.

10. van de Donk NWCJ, Moreau P, Garfall AL, et al. Long-term follow-up from MajesTEC-1 of teclistamab, a B-cell maturation antigen (BCMA) x CD3 bispecific antibody, in patients with relapsed/refractory multiple myeloma (RRMM). J Clin Oncol. 2023;41(Suppl 16):S8011.

11. Li H, van der Leun AM, Yofe I, et al. Dysfunctional CD8 T cells form a proliferative, dynamically regulated compartment within human melanoma. Cell. 2019;176(4):775-789.e18.

12. Friedrich MJ, Neri P, Kehl N, et al. The pre-existing T cell landscape determines the response to bispecific T cell engagers in multiple myeloma patients. Cancer Cell. 2023;41(4):711-725.e6.

13. Cortes-Selva D, Perova T, Skerget S, et al. Correlation of immune fitness with response to teclistamab in relapsed/refractory multiple myeloma in the MajesTEC-1 study. Blood. 2024;144(6):615-628.

14. Cohen YC, Magen H, Gatt M, et al. Talquetamab plus teclistamab in relapsed or refractory multiple myeloma. N Engl J Med. 2025;392(2):138-149.

15. Costa LJ, Bahlis NJ, Perrot A, et al. Teclistamab plus daratumumab in relapsed or refractory multiple myeloma. N Engl J Med. 2026;394(8):739-752.

16. Moreau P, Garfall AL, van de Donk N, et al. Teclistamab in relapsed or refractory multiple myeloma. N Engl J Med. 2022;387(6):495-505.

17. Usmani SZ, Garfall AL, van de Donk N, et al. Teclistamab, a B-cell maturation antigen x CD3 bispecific antibody, in patients with relapsed or refractory multiple myeloma (MajesTEC-1): a multicentre, open-label, single-arm, phase 1 study. Lancet. 2021;398(10301):665-674.

18. Kumar S, Paiva B, Anderson KC, et al. International Myeloma Working Group consensus criteria for response and minimal residual disease assessment in multiple myeloma. Lancet Oncol. 2016;17(8):e328-e346.

19. Rajkumar SV, Harousseau JL, Durie B, et al. Consensus recommendations for the uniform reporting of clinical trials: report of the International Myeloma Workshop Consensus Panel 1. Blood. 2011;117(18):4691-4695.

20. Abraham Y, Neri M. HilbertSimilarity : estimating sample similarity in single cell high dimensional datasets (0.4.3).Available at https://zenodo.org/record/3557362#.YmayIdrMJPY Accessed April 16, 2026.

21. Qiu P. Inferring phenotypic properties from single-cell characteristics. PLoS One. 2012;7(5):e37038.

22. Diggins KE, Greenplate AR, Leelatian N, Wogsland CE, Irish JM. Characterizing cell subsets using marker enrichment modeling. Nat Methods. 2017;14(3):275-278.

23. Pedersen CB, Dam SH, Barnkob MB, et al. cyCombine allows for robust integration of single-cell cytometry datasets within and across technologies. Nat Commun. 2022;13(1):1698.

24. Van Gassen S, Callebaut B, Van Helden MJ, et al. FlowSOM: Using self-organizing maps for visualization and interpretation of cytometry data. Cytometry A. 2015;87(7):636-645.

25. Demsar J, Leban G, Zupan B. FreeViz--an intelligent multivariate visualization approach to explorative analysis of biomedical data. J Biomed Inform. 2007;40(6):661-671.

26. Verkleij CPM, O'Neill CA, Broekmans MEC, et al. T-cell characteristics impact response and resistance to T-cell-redirecting bispecific antibodies in multiple myeloma. Clin Cancer Res. 2024;30(14):3006-3022.

27. Krejcik J, Casneuf T, Nijhof IS, et al. Daratumumab depletes $CD38^+$ immune regulatory cells, promotes T-cell expansion, and skews T-cell repertoire in multiple myeloma. Blood. 2016;128(3):384-394.

28. ClinicalTrials.gov. A study of JNJ-79635322 in participants with relapsed or refractory multiple myeloma or previously treated Amyloid Light-chain (AL) Amyloidosis. Available at https://clinicaltrials.gov/study/NCT05652335 Accessed December 11, 2025.

29. Broske AE, Korfi K, Belousov A, et al. Pharmacodynamics and molecular correlates of response to glofitamab in relapsed/refractory non-Hodgkin lymphoma. Blood Adv. 2022;6(3):1025-1037.

30. O'Brien N, Mueller JPJ, Broske AE, et al. T cell margination: investigating the detour of T cells following forimtamig treatment in humanized mice. MAbs. 2025;17(1):2440578.

31. Lee H, Neri P, Bahlis NJ. Current use of bispecific antibodies to treat multiple myeloma. Hematology Am Soc Hematol Educ Program. 2023;2023(1):332-339.

32. Malavasi F, Deaglio S, Funaro A, et al. Evolution and function of the ADP ribosyl cyclase/CD38 gene family in physiology and pathology. Physiol Rev. 2008;88(3):841-886.

33. Chen X, Ghanizada M, Mallajosyula V, et al. Differential roles of human CD4(+) and CD8(+) regulatory T cells in controlling self-reactive immune responses. Nat Immunol. 2025;26(2):230-239.

34. Cotner T, Williams JM, Christenson L, Shapiro HM, Strom TB, Strominger J. Simultaneous flow cytometric analysis of human T cell activation antigen expression and DNA content. J Exp Med. 1983;157(2):461-472.

35. Sandoval-Montes C, Santos-Argumedo L. CD38 is expressed selectively during the activation of a subset of mature T cells with reduced proliferation but improved potential to produce cytokines. J Leukoc Biol. 2005;77(4):513-521.

36. Long Q, Song S, Xue J, et al. The CD38(+)HLA-DR(+) T cells with activation and exhaustion characteristics as predictors of severity and mortality in COVID-19 patients. Front Immunol. 2025;16:1577803.

37. Gunasinghe SD, Peres NG, Goyette J, Gaus K. Biomechanics of T cell dysfunctions in chronic diseases. Front Immunol. 2021;12:600829.

38. Hofmann M, Thimme R, Schamel WW. PD-1 and LAG-3: synergistic fostering of T cell exhaustion. Signal Transduct Target Ther. 2024;9(1):291.

39. Verkleij CPM, Broekmans MEC, van Duin M, et al. Preclinical activity and determinants of response of the GPRC5DxCD3 bispecific antibody talquetamab in multiple myeloma. Blood Adv. 2021;5(8):2196-2215.

40. Duell J, Dittrich M, Bedke T, et al. Frequency of regulatory T cells determines the outcome of the T-cell-engaging antibody blinatumomab in patients with B-precursor ALL. Leukemia. 2017;31(10):2181-2190.

41. Feng X, Zhang L, Acharya C, et al. Targeting CD38 suppresses induction and function of T regulatory cells to mitigate immunosuppression in multiple myeloma. Clin Cancer Res. 2017;23(15):4290-4300.

42. Manna A, Kellett T, Aulakh S, et al. Targeting CD38 is lethal to Breg-like chronic lymphocytic leukemia cells and Tregs, but restores CD8+ T-cell responses. Blood Adv. 2020;4(10):2143-2157.

43. Huang Y, Zheng H, Zhu Y, et al. Loss of CD28 expression associates with severe T-cell exhaustion in acute myeloid leukemia. Front Immunol. 2023;14:1139517.

44. Xia Y, Shen X, Shi M, et al. Tigit: the potential mechanisms of relapse in multiple myeloma following anti-BCMA CAR-T therapy and a promising target for improving CAR-T efficacy. Blood. 2024;144(Supplement 1):2033.

45. Asimakopoulos F. TIGIT checkpoint inhibition for myeloma. Blood. 2018;132(16):1629-1630.

46. Lee H, Durante M, Skerget S, et al. Impact of soluble BCMA and non-T-cell factors on refractoriness to BCMA-targeting T-cell engagers in multiple myeloma. Blood. 2024;144(25):2637-2651.

47. Lee H, Ahn S, Maity R, et al. Mechanisms of antigen escape from BCMA- or GPRC5D-targeted immunotherapies in multiple myeloma. Nat Med. 2023;29(9):2295-2306.

Figure Legends

Figure 1. Absolute counts of CD4+ and CD8+ T cells in the periphery of responders versus nonresponders. (A) Changes in absolute counts of CD4+ T cells following administration of the first step-up dose (SUD1) of teclistamab. (B) Changes in absolute counts of CD8+ T cells following administration of SUD1 of teclistamab; 4 data points are not shown to improve clarity of the y axis and aid in data visualization (data points were retained in the dataset and included in all statistical analyses). Red outlines indicate T cell margination occurring within 24 hours after administration of SUD1; blue outlines indicate T cell recovery after the first full treatment. (C) Maximum fold change (max FC) from SUD1_PRE to SUD1_24H for CD4+ T cells. (D) max FC from SUD1_PRE to SUD1_24H for CD8+ T cells. (E) Max FC from SUD1_24H to C3D1_PRE for CD4+ T cells. (F) max FC from SUD1_24H to C3D1_PRE for CD8+ T cells. Max FC was calculated per patient. Data are presented as box plots showing median and interquartile ranges. Statistical significance was assessed using the Wilcoxon rank-sum test, **P*<0.05, ****P*<0.001. C, Cycle; D, Day; PRE, predose.

Figure 2. Longitudinal expression and maximum fold change of CD38+ on CD8+ T cells. (A) Longitudinal expression of CD38+ CD8+ T cells in the peripheral blood following administration of first step-up dose (SUD1) of teclistamab. (B) Maximum fold change (max FC) induction of CD38 expression on CD8+ T cells from baseline to C2D1; 2 data points are not shown to improve clarity of the y axis and aid in data visualization (data points were retained in the dataset and included in all statistical analyses). Max FC was calculated per patient. Data are presented as box plots showing median and interquartile ranges. Statistical significance was assessed using the Wilcoxon rank-sum test, **P*<0.05. C, Cycle; D, Day; PRE, predose.

Figure 3. Longitudinal expression of coinhibitory checkpoint markers on CD8+ T cells in the peripheral blood of responders versus nonresponders. (A) Lymphocyte activation gene-3 (LAG-3) on CD8+ T cells; 6 data points are not shown to improve clarity of the y axis and aid in data visualization (data points were retained in the dataset and included in all statistical analyses). (B) T cell immunoglobulin mucin-3 (TIM-3) on CD8+ T cells; 20 data points are not shown to improve clarity of the y axis and aid in data visualization (data points were retained in the dataset and included in all statistical analyses). (C) Programmed death-1 (PD-1) on CD8+ T cells. (D) PD-1/TIM-3 on CD8+ T cells; 10 data points are not shown to improve clarity of the y axis and aid in data visualization (data points were retained in the dataset and included in all statistical analyses). (E) PD-1/LAG-3 on CD8+ T cells; 4 data points are not shown to improve clarity of the y axis and aid in data visualization (data points were retained in the dataset and included in all statistical analyses). Data are presented as box plots showing median and interquartile ranges. Statistical significance at SUD1_PRE and C3D1_PRE was assessed using the Wilcoxon rank-sum test, *P<0.05, **P<0.01 ***P<0.001. C, Cycle; D, Day; PRE, predose; SUD1, step-up dose 1.

Figure 4. Proportions of regulatory T cells and CD38+ regulatory T cells in the peripheral blood of responders versus nonresponders. (A) The longitudinal proportion of immunosuppressive regulatory T cells (Tregs) following administration of first step-up dose (SUD1) of teclistamab. (B) The longitudinal proportion of CD38-expressing Tregs following administration of SUD1 of teclistamab; 6 data points are not shown to improve clarity of the y axis and aid in data visualization (data points were retained in the dataset and included in all statistical analyses). Data are presented as box plots showing median and interquartile ranges. Statistical significance at SUD1_PRE and C3D1_PRE was assessed using the Wilcoxon rank-sum test, *P<0.05. C, Cycle; D, Day; PRE, predose.

Figure 5. Longitudinal expression of coinhibitory receptors on CD4+ and CD8+ T cells, and CD3+ T cells in the bone marrow of responders versus nonresponders. (A) Longitudinal proportion of CD3+ T cells; 7 data points are not shown to improve clarity of the y axis and aid in data visualization (data points were retained in the dataset and included in all statistical analyses). (B) Longitudinal expression of programmed death-1 (PD-1) on CD4+ T cells and (C) on CD8+ T cells following administration of first step-up dose (SUD1) of teclistamab. (D) Longitudinal expression of T cell immunoglobulin mucin-3 (TIM-3) on CD4+ T cells. (E) Longitudinal expression of TIM-3 on CD8+ T cells. (F) Longitudinal expression of PD-1/TIM-3 on CD4+ T cells; 3 data points are not shown to improve clarity of the y axis and aid in data visualization (data points were retained in the dataset and included in all statistical analyses). (G) Longitudinal expression of PD-1/TIM-3 on CD8+ T cells. Data are presented as box plots showing median and interquartile ranges. Statistical significance was assessed using the Wilcoxon rank-sum test, **P*<0.05, ***P*<0.01,****P*<0.001. C, Cycle; D, Day; PRE, predose.

Figure 6. Changes in the CD8+ and CD4+ T cell composition at relapse in the peripheral blood identified using polyfunctional analysis by CyTOF. Peripheral blood (PB) samples from 25 patients treated with teclistamab were collected at baseline and at progressive disease (PD) for T cell profiling by CyTOF (cytometry by time of flight). FreeViz visualizations and polyfunctionality analysis were used to explore shifts in the composition of CD8+ and CD4+ T cell metaclusters, identified by FlowSOM, at PD, relative to baseline. Cell distributions were visualized using contour plots for baseline (blue lines) and PD (red lines) samples. For clarity, markers enclosed in boxes represent those that overlap within the FreeViz visualization. The placement of these boxed markers is intended solely to display hidden/overlapping labels and does not carry any biological interpretation. Fan plots were used to visualize the expression of all markers in depleted, enriched and unchanged (ie, reference) populations. (A) FreeViz projection of PB CD8+ T cells. (B) FreeViz projection of PB CD4+ T cells. Bins (cell subsets)

enriched at PD (red circles) were representative of CD8+ T cells (A) or CD4+ T cells (B) expressing markers of senescence and exhaustion, as confirmed by the fan plot visualization of all markers used for the analysis.

BCMA, B-cell maturation antigen; CCR4, chemokine receptor type 4; Eomes, eomesodermin; GPRC5D, G protein-coupled receptor class C group 5 member D; HLA-DR, human leukocyte antigen – DR isotype; KLRG1, killer cell lectin-like receptor G1; LAG-3, lymphocyte activation gene-3 (CD233); NK, natural killer; PD-1, programmed death-1 (CD279); T-bet, T-box expressed in T-cells; TIGIT, T cell immunoreceptor with immunoglobulin and immunoreceptor tyrosine-based inhibitory motif domain; TIM-3, T cell immunoglobulin mucin-3 (CD366); TOX, thymocyte selection-associated high mobility group box.

Figure 7. Changes in the CD8+ and CD4+ T cell composition at relapse in the bone marrow identified using polyfunctional analysis by CyTOF. Bone marrow (BM) samples from 23 patients treated with teclistamab were collected at baseline and at progressive disease (PD) for T cell profiling by CyTOF (cytometry by time of flight). FreeViz visualizations and polyfunctionality analysis were used to explore shifts in the composition of CD8+ and CD4+ T cell metaclusters, identified by FlowSOM, at PD, relative to baseline. Cell distributions were visualized using contour plots for baseline (blue lines) and PD (red lines) samples. For clarity, markers enclosed in boxes represent those that overlap within the FreeViz visualization. The placement of these boxed markers is intended solely to display hidden/overlapping labels and does not carry any biological interpretation. Fan plots were used to visualize the expression of all markers in depleted, enriched and unchanged (ie, reference) populations. (A) FreeViz projection of BM CD8+ T cells. (B) FreeViz projection of BM CD4+ T cells. Bins (cell subsets) enriched at PD (red circles) were representative of CD8+ T cells (A) or CD4+ T cells (B) expressing markers of senescence, exhaustion, and terminal differentiation, as confirmed by the fan plot visualization of all markers used for the analysis.

BCMA, B-cell maturation antigen; CCR4, chemokine receptor type 4; Eomes, eomesodermin; GPRC5D, G protein-coupled receptor class C group 5 member D; HLA-DR, human leukocyte antigen – DR isotype; KLRG1, killer cell lectin-like receptor G1; LAG-3, lymphocyte activation gene-3 (CD233); NK, natural killer; PD-1, programmed death-1 (CD279); T-bet, T-box expressed in T-cells; TIGIT, T cell immunoreceptor with immunoglobulin and immunoreceptor tyrosine-based inhibitory motif domain; TIM-3, T cell immunoglobulin mucin-3 (CD366); TOX, thymocyte selection-associated high mobility group box.

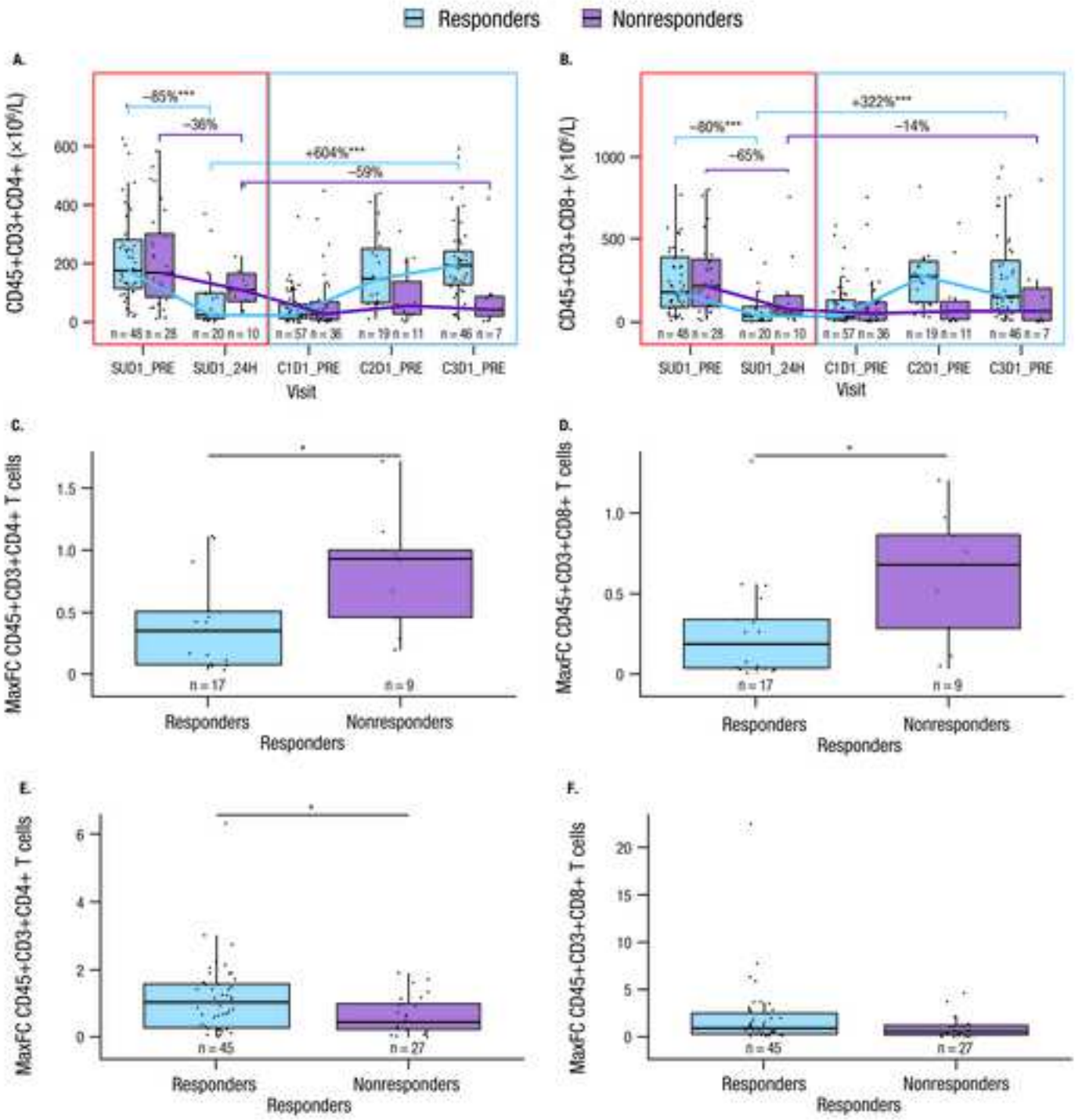
Responders
Nonresponders
A.
CD45+CD3+CD4+ (×10⁶/L)
−65%***
−36%
+604%***
−59%
n = 46 n = 28
n = 20 n = 10
n = 57 n = 36
n = 19 n = 11
n = 46 n = 7
SU01_PRE
SU01_24H
C1D1_PRE
C2D1_PRE
C3D1_PRE
Visit
B.
CD45+CD3+CD8+ (×10⁶/L)
−80%***
+322%***
−65%
−14%
Visit
C.
MaxFC CD45+CD3+CD4+ T cells
n = 17
n = 9
Responders
Nonresponders
Responders
D.
MaxFC CD45+CD3+CD8+ T cells
E.
MaxFC CD45+CD3+CD4+ T cells
n = 45
n = 27
F.
MaxFC CD45+CD3+CD8+ T cells

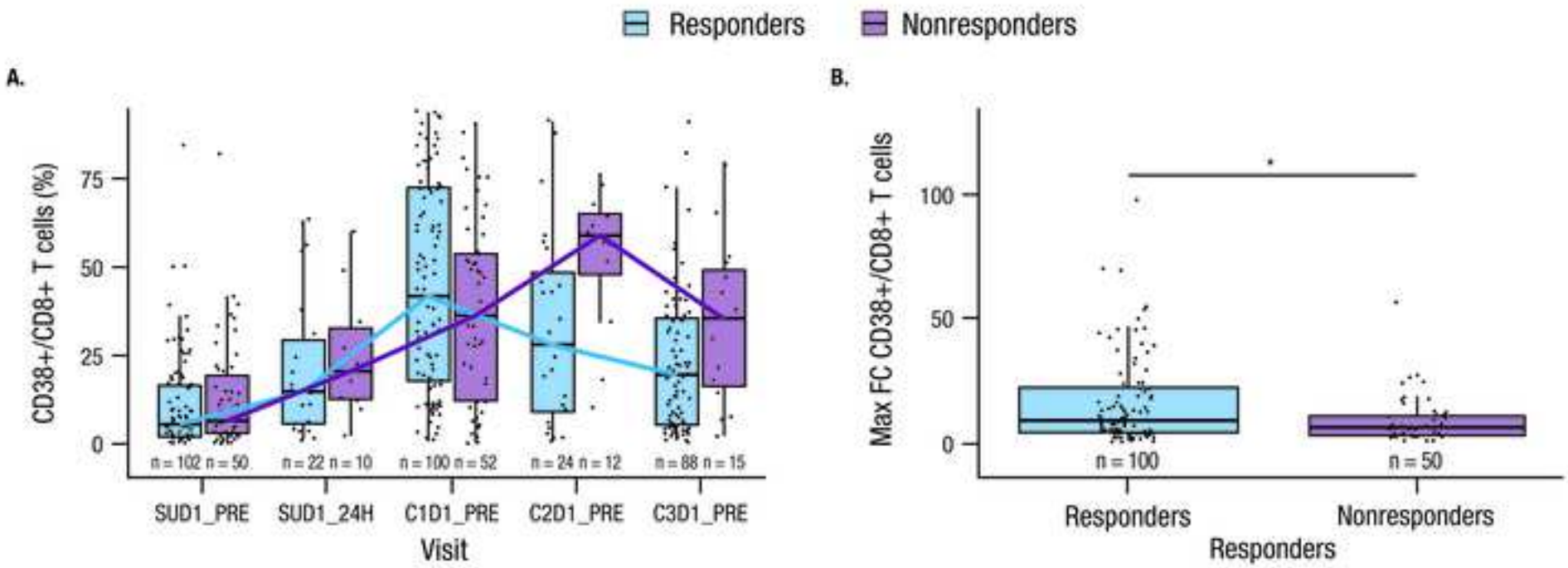
Responders
Nonresponders
A.
CD38+/CD8+ T cells (%)
75
50
25
0
n = 102 n = 50
n = 22 n = 10
n = 100 n = 52
n = 24 n = 12
n = 88 n = 15
SUD1_PRE
SUD1_24H
C1D1_PRE
C2D1_PRE
C3D1_PRE
Visit
B.
Max FC CD38+/CD8+ T cells
100
50
0
n = 100
n = 50
Responders
Nonresponders
Responders

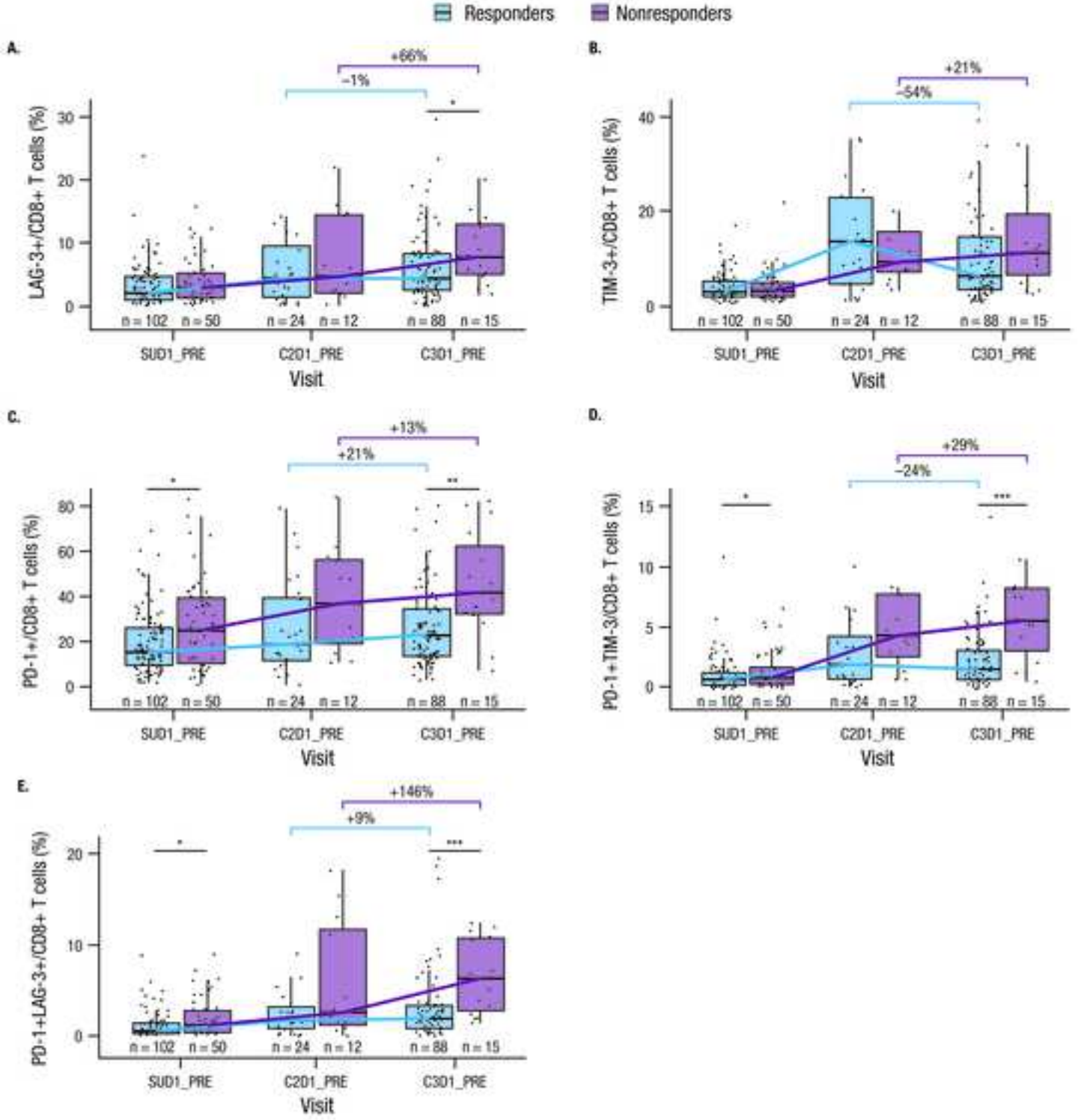
Responders
Nonresponders
A.
LAG-3+/CD8+ T cells (%)
+66%
−1%
B.
TIM-3+/CD8+ T cells (%)
+21%
−54%
C.
PD-1+/CD8+ T cells (%)
+13%
+21%
D.
PD-1+TIM-3/CD8+ T cells (%)
+29%
−24%
E.
PD-1+LAG-3+/CD8+ T cells (%)
+146%
+9%
n = 102
n = 50
n = 24
n = 12
n = 88
n = 15
SUD1_PRE
C2D1_PRE
C3D1_PRE
Visit

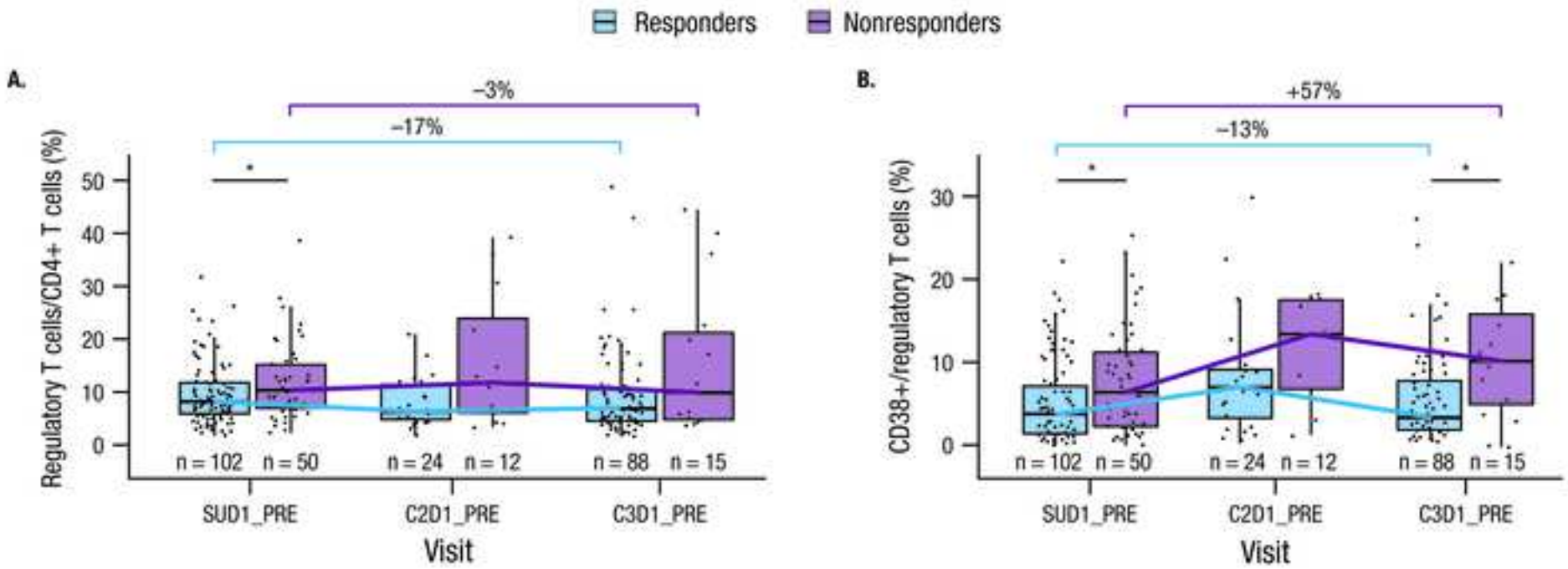
Responders
Nonresponders
A.
−3%
−17%
*
Regulatory T cells/CD4+ T cells (%)
50
40
30
20
10
0
n = 102
n = 50
n = 24
n = 12
n = 88
n = 15
SUD1_PRE
C2D1_PRE
C3D1_PRE
Visit
B.
+57%
−13%
*
*
CD38+/regulatory T cells (%)
30
20
10
0
n = 102
n = 50
n = 24
n = 12
n = 88
n = 15
SUD1_PRE
C2D1_PRE
C3D1_PRE
Visit

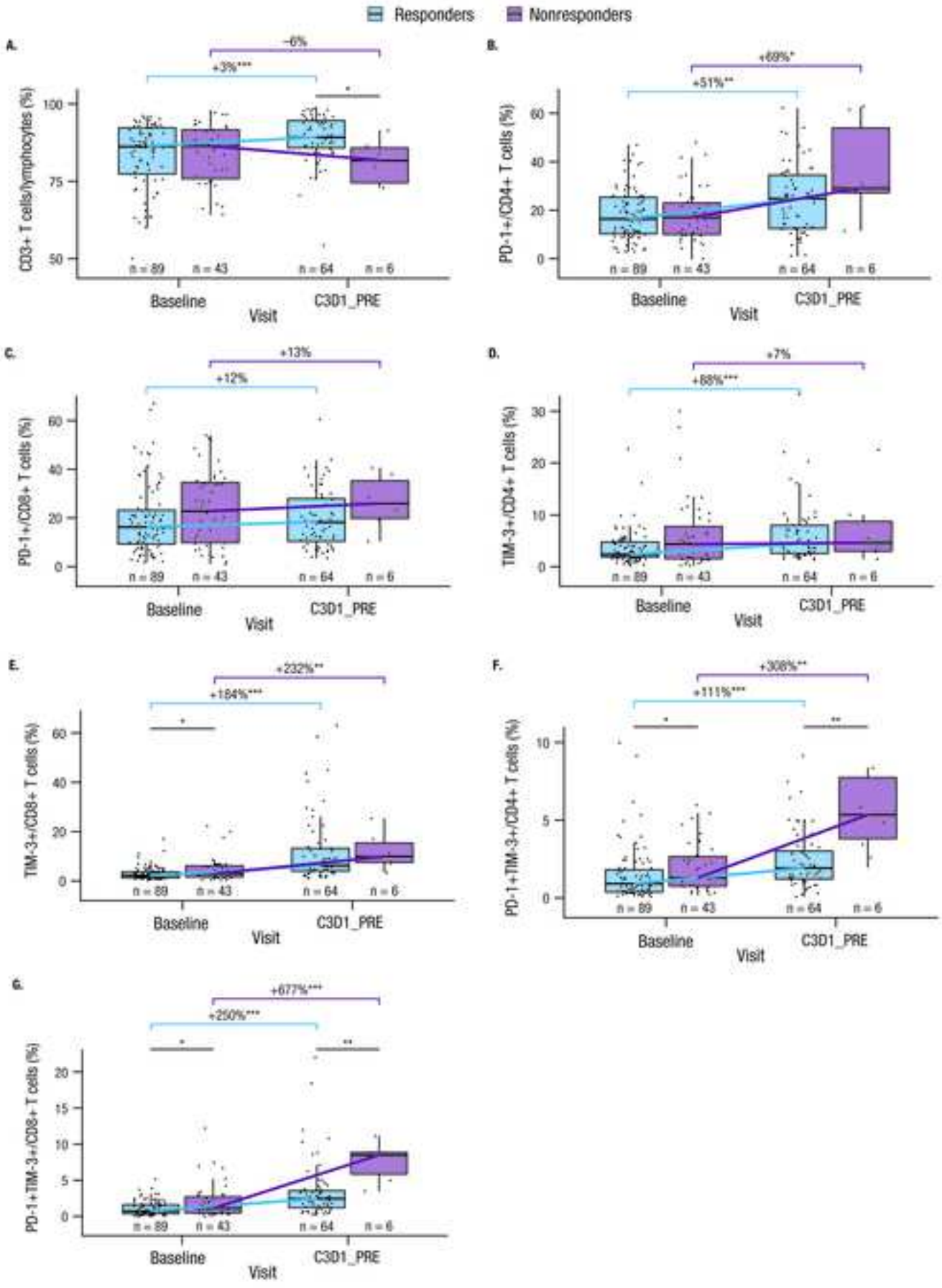
Responders
Nonresponders
A.
−6%
+3%***
CD3+ T cells/lymphocytes (%)
B.
+69%*
+51%**
PD-1+/CD4+ T cells (%)
C.
+13%
+12%
PD-1+/CD8+ T cells (%)
D.
+7%
+68%***
TIM-3+/CD4+ T cells (%)
E.
+232%**
+184%***
TIM-3+/CD8+ T cells (%)
F.
+308%**
+111%***
PD-1+TIM-3+/CD4+ T cells (%)
G.
+677%***
+250%***
PD-1+TIM-3+/CD8+ T cells (%)
n = 89
n = 43
n = 64
n = 6
Baseline
C3D1_PRE
Visit

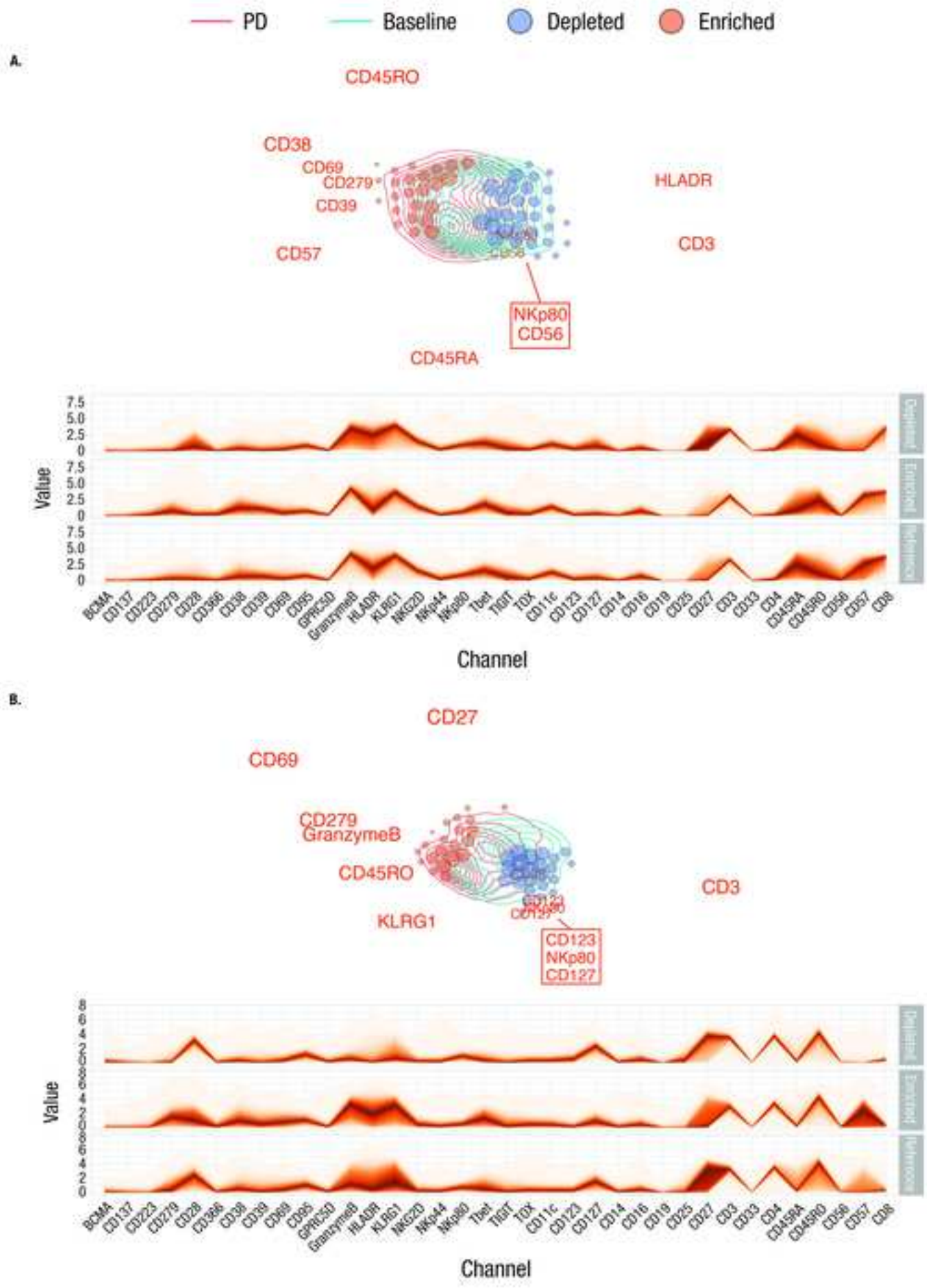
PD
Baseline
Depleted
Enriched
A.
CD45RO
CD38
CD69
CD279
CD39
CD57
HLADR
CD3
NKp80
CD56
CD45RA
Value
Channel
B.
CD27
CD69
CD279
GranzymeB
CD45RO
KLRG1
CD3
CD123
NKp80
CD127
Value
Channel

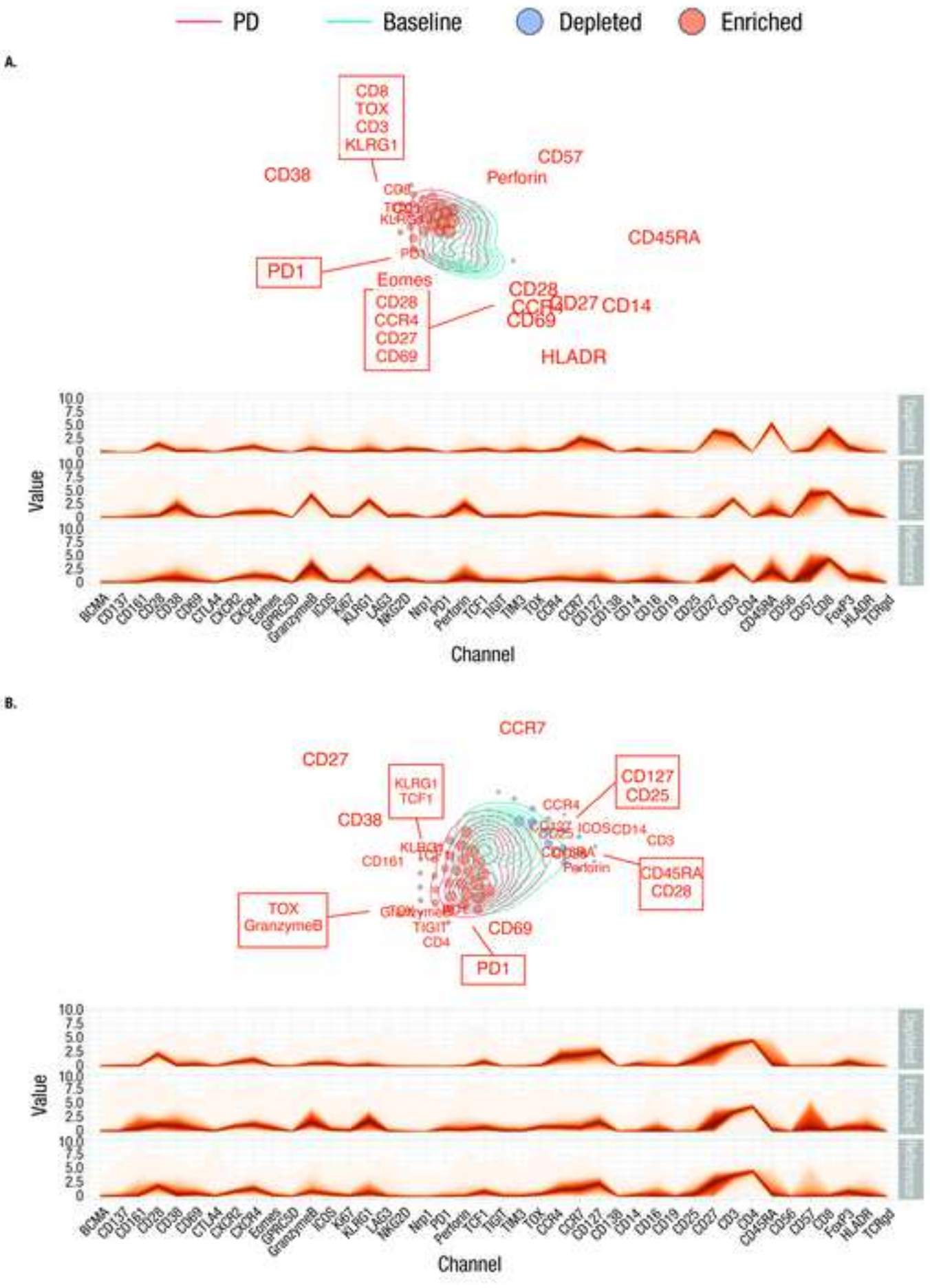
PD
Baseline
Depleted
Enriched
A.
CD8
TOX
CD3
KLRG1
CD57
CD38
Perforin
CD45RA
PD1
Eomes
CD28
CCR4
CD27
CD69
CD14
HLADR
Value
Channel
B.
CCR7
CD27
KLRG1
TCF1
CD127
CD25
CD38
CCR4
ICOS
CD14
CD3
CD161
Perforin
CD45RA
CD28
TOX
GranzymeB
TIGIT
CD4
CD69
PD1
Value
Channel

Supplemental Material

Longitudinal mechanisms of response, resistance and relapse to teclistamab in multiple myeloma: results from MajesTEC-1

Deeksha Vishwamitra,[1] Sheri Skerget,[1] Diana Cortes-Selva,[1] Tatiana Perova,[1] Onsay Lau,[1] Cuc Davis,[1] Rengasamy Boominathan,[1] Jaymala Patel,[1] Koen Van den Berge,[2] Yue Guo,[1] Xin Miao,[1] Tara Stephenson,[1] Caroline Hodin,[2] Clarissa Uhlar,[1] Lixia Pei,[3] Danielle Trancucci,[3] Athena F Zuppa,[3] Katherine Chastain,[3] Arnob Banerjee,[1] Rachel Kobos,[3] Nizar J Bahlis,[4] Niels WCJ van de Donk,[5] and Raluca I Verona[1]

[1]Johnson & Johnson, Spring House, PA, USA; [2]Johnson & Johnson, Beerse, Belgium; [3]Johnson & Johnson, Raritan, NJ, USA; [4]Arnie Charbonneau Cancer Institute, University of Calgary, Calgary, AB, Canada; and [5]Amsterdam University Medical Center, Vrije Universiteit Amsterdam, Amsterdam, The Netherlands

SUPPLEMENTAL APPENDIX

Methods

Study design and patient population

MajesTEC-1 is an ongoing, phase 1/2, open-label, multicenter clinical trial assessing the efficacy of teclistamab for the treatment of patients with relapsed/refractory multiple myeloma (RRMM) who have received ≥3 prior lines of therapy, including ≥1 proteasome inhibitor, 1 immunomodulatory drug (IMiD), and 1 anti-CD38 monoclonal antibody.[1,2] Key eligibility criteria included age ≥18 years, documented multiple myeloma (MM) diagnosis per International Myeloma Working Group (IMWG) criteria,[3,4] measurable disease at screening, and an Eastern Cooperative Oncology Group performance status score of 0 or 1.

The pivotal recommended phase 2 dose cohort comprised 165 patients who received subcutaneous teclistamab 1.5 mg/kg weekly, following step-up doses (0.06 mg/kg and 0.3 mg/kg). Treatment with teclistamab continued once weekly until disease progression, unacceptable toxicity, withdrawal of consent, or death, whichever occurred first. Patients were allowed to switch to less frequent dosing (once every 2 weeks) if they achieved at least a partial response (≥PR) for a minimum of 4 cycles during phase 1, or a complete response or better for ≥6 months in phase 2. For the purpose of this analysis, teclistamab responders were defined as patients who achieved a best clinical response of ≥PR per IMWG criteria,[3,4] as assessed by an independent review committee; patients who did not achieve this were considered nonresponders. Patients who responded and then progressed had a best response of ≥PR and were classified as having progressive disease per independent review committee assessment. Confirmed disease progression (per IMWG criteria) was a per-protocol reason for discontinuation of study treatment.

Analyses of bone marrow and peripheral blood samples using flow cytometry

Peripheral blood was collected prior to step-up dose 1 (baseline) and at various longitudinal timepoints and bone marrow samples analyzed by flow cytometry were collected at baseline and at Cycle (C) 3 Day (D) 1, and progressive disease (PD).

Baseline and PD proportions and density of membrane-bound B-cell maturation antigen (BCMA) was performed using CD138+ enriched plasma cells from bone marrow by staining with the following antibodies: CD45 (clone: 2D1, BD Biosciences), fixable viability dye eFluor506 (eBiosciences), CD38 (clone: Humab-003, Johnson & Johnson), CD138 (DL-101, Biolegend), and CD269 BCMA (clone: 19F2, Biolegend). Receptor density assessment was performed using AF647 Quantum beads (Bang Laboratories).

Immunophenotyping was performed in a BD FACSCelesta (BD Biosciences), and data were analyzed in FlowJo (V10.6.2). Measurement of immune markers in T cells from peripheral blood and bone marrow mononuclear cells (isolated using Ficoll Paque PREMIUM density gradient centrifugation) was performed using the following antibodies: CD38 (Humab-003, Johnson & Johnson), PD-1 (EH12.1, BD Biosciences), TIM-3 (7D3, BD Biosciences), LAG-3 (3DS223H, ThermoFisher), CD3 (UCHT1, BD Biosciences), CD4 (RPA-T4, BD Biosciences), CD8 (SK1, BD Biosciences), CD127 (eBioRDR5, ThermoFisher), CD45RA (HI100, BD Biosciences), CD45RO (UCHL1, BD Biosciences), and eFluor506 Fixable Viability Dye (ThermoFisher) to assess viability. To prevent nonspecific binding of antibodies, a Fc-blocking reagent (FC Block, ThermoFisher) was added. Sample acquisition was performed in a BD LSR Fortessa X-20 (Becton Dickinson) cytometer. Quantitation of cell populations was performed using an off-the-shelf TBNK kit assay (BD Biosciences) and T cell activation assay (BD Biosciences of

ThermoFisher) according to the manufacturer's instructions. Immunosuppressive regulatory T cells were defined as CD3+CD4+CD25hiCD127dim

Analyses of bone marrow and peripheral blood samples using cytometry by time of flight (CyTOF)

Peripheral blood samples were collected and fixed in Smart Tubes® (Smart Tube, Inc.) according to manufacturer's instructions. CyTOF profiling was evaluated from active dose cohorts. Peripheral blood samples from 25 patients were collected at baseline and at relapse (38 samples in total [23 samples from screening and 15 samples from relapse]). Additionally, bone marrow samples collected at baseline from 23 patients who relapsed were profiled using CyTOF (34 samples in total [20 samples from screening and 14 samples from relapse]). For bone marrow samples, CD138-depleted, fraction-viable, cryopreserved bone marrow samples were used.

Two panels of 40 and 44 antibodies were used for analysis of the peripheral blood and bone marrow samples, respectively (**Supplemental Tables 1** and **2**). Antibodies pre-conjugated to metal isotopes were purchased from Standard BioTools. Additional antibodies were purchased from other vendors and conjugated to metal isotopes using the Maxpar® Antibody Labeling Kit (Standard Bio Tools) according to the manufacturer's protocol.

The frozen Smart Tube whole blood samples were thawed in a water bath at 10°C for 20 minutes, then 3 mL of 1 × Thaw-Lyse buffer (Smart Tube) was added, mixed, and strained through a 70-µM strainer (MACS SmartStrainer, Miltenyi Biotec Inc.). The strainer was washed with 40 mL of 1 × Thaw-Lyse buffer and incubated at room temperature for 10 minutes for lysing red blood cells. The samples were centrifuged (600 g, 5 minutes, 20°C), and pellets were resuspended in 1 × BD lysing buffer (BD Biosciences) and incubated for 10 minutes at room

temperature for additional red blood lysis. After centrifugation, the pellets were resuspended in 100 µL of stain buffer, and the samples were purified using CD235 microbeads for negative selection, a method in accordance with the manufacturer's protocol, and incubated for 30 minutes at room temperature. After purification, the samples were centrifuged (600 g, 5 minutes, 20°C) and washed with stain buffer. Then, the samples were incubated with TruStain FcX (BioLegend) for 30 minutes at room temperature to block surface Fc receptors. After washing off the TruStain FcX blocker, the cells were stained with a mixture of surface antibodies and incubated at room temperature for 30 minutes. Cells were washed with staining buffer, resuspended in BD transcription factor fix and perm buffer (BD Pharmingen), and incubated at 4°C for 45 minutes. After incubation, cells were washed twice with 1 × BD Perm/Wash buffer (BD Pharmingen), resuspended in the intracellular staining antibody mixture, and incubated at 4°C for 45 minutes. After washing with 1 × BD Perm/Wash buffer, the cell pellets were resuspended in phosphate-buffered saline with saponin (0.3%) containing formaldehyde (1.6%) and 125 nM Ir intercalator (Cell-ID™ Intercalator-Ir–125 µM, Standard Bio Tools) and incubated at 4°C overnight.

Bone marrow (frozen viable) samples, depleted of CD138+ cells, were thawed and immediately transferred to 5 mL of media and centrifuged. After centrifugation and 15-minute TruStain FcX incubation, washing and surface-staining incubation for 35 minutes was performed. Samples were then barcoded using the Standard Bio Tools Cell-ID 20-Plex Pd barcoding kit. This step was included to minimize cell loss and reduce technical variability during intracellular staining. After barcoding, samples were pooled, and intracellular staining using a transcription factor buffer set (BD Biosciences) was performed according to the manufacturer's instructions. After washing, cell pellets were resuspended in phosphate-buffered saline with saponin (0.3%)

containing formaldehyde (1.6%) and 50 nM Ir intercalator (Cell-ID™) and incubated at 4°C overnight.

After overnight incubation, stained cells were washed with a staining buffer and subsequently washed in a Maxpar Cell Acquisition Solution (Standard Bio Tools) to remove buffer salts. Cells were then resuspended in a Maxpar Cell Acquisition Solution with a 1:10 dilution of EQ Four Element Calibration beads (Standard Bio Tools) and filtered through a 35-µm nylon mesh filter cap (Falcon). Samples were analyzed on a Helios CyTOF mass cytometer (Standard BioTools). Each experimental batch included peripheral blood mononuclear cells (PBMC) samples from 2 healthy donors as quality controls used to monitor possible technical (batch-to-batch) variability associated with sample processing, staining, and acquisition on different days. In total, peripheral blood samples were analyzed in 11 batches, while bone marrow samples were processed in 3 batches.

CyTOF data acquisition and normalization

Data acquired on CyTOF were obtained in flow cytometry standard (fcs) file format and normalized using CyTOF software 7.0.8493 for Stand-Alone Processing Workstations (Standard BioTools). Of note, data for pooled bone marrow samples were computationally de-barcoded using CyTOF software to generate individual sample-specific files for analysis. Manual gating of immune populations was performed in Cytobank software v10.2 (Beckman Coulter). Samples with >10,000 live CD45+CD66b– singlet events were included in the unsupervised analysis. A hypothesis-generating approach was then applied to detect data trends using in-house scripts in R 4.0.2, as further detailed in following sections.

CyTOF quality control and batch effect correction

Quality control for peripheral blood and bone marrow was performed using the HilbertSimilarity distance (distance measure between samples, based on discretized marker expression),[5] Earth Mover's distance (distance measure between samples, based on self-organizing maps [SOM] using FlowSOM clustering),[6] and marker enrichment modeling algorithms (assessing marker intensity distributions).[7] These metrics assessed potential batch effects at the sample, cluster, and marker levels, respectively, as well as the overall quality of the samples and marker staining. CyTOF data were generated and processed in different batches, introducing technical variation as measured using the above quality metrics. This variation was corrected using cyCombine v0.2.16 (Github biosurg/cyCombine@b0904f1)[8] with the following parameters: grid size of 8 × 8, normalization method scale, seed 2023 for peripheral blood data, and seed 2024 for bone marrow data, as described.[8] Briefly, all cells in the dataset were clustered in a 8x8 SOM grid to obtain clusters of phenotypically similar cells. Then batch correction was applied to each cluster of cells separately based on the empirical bayes model of ComBAT. Effectiveness of the correction was confirmed using HilbertSimilarity distance and Earth Mover's Distance, and parameters were optimized based on these metrics. Control-sample clustering was also used to confirm appropriate correction where needed.

Cell clustering and annotation

FlowSOM 2.1.4[9] was applied to the corrected, normalized data with a grid size of 18 × 18, generating multiple clusters subsequently grouped into 30 metaclusters. Marker expression, corresponding to median metal intensity, in each metacluster was manually reviewed to identify known immune-cell subsets, and subpopulations were further refined and annotated.

Polyfunctionality analysis

CD4 and CD8 T cell subsets identified via FlowSOM metacluster annotation were visualized using FreeViz.[10] Functional and phenotypic markers (see **Supplemental Table 1 and 2** for details on each marker) were positioned as anchors in the FreeViz space to maximize the separation between treatment timepoints (baseline and disease progression) as described,[10] and density plots displayed composition shifts. Fan charts[11] showed marker centiles per condition using stacked area plots with peak intensity at the 50th centile; details have been previously described.[12,13]

The FreeViz space was divided into 12 × 12 (144) bins using a SOM on a downsampled dataset (downsampling strategy: divide the 2D FreeViz space into cubes using the hilbertSimilarity methods[5] [16 cuts in each dimension], and down/up-sample 100 cells from each non-empty cube), and these bins were then applied to the full dataset to obtain per-sample cell counts. Counts were centered log-ratio (clr) transformed, and a linear mixed model (clr ~ condition + batchID + [1|individual]) was fitted. Contrasts were calculated using estimated marginal means, and the p-values were corrected across the SOM bins using Benjamini-Hochberg method. Bins were colored to reflect differential abundance (enrichment or depletion) in the FreeViz space.

Baseline serum soluble BCMA quantitation

Serum was collected prior to the first teclistamab dose (baseline) and at PD. Serum samples were analyzed for soluble BCMA using an electrochemiluminescence ligand-binding assay using the Meso Scale Discovery (MSD) platform. Briefly, the assay used a biotin-labeled, antihuman BCMA antibody and a Sulfo-tag (ruthenium)–labeled antihuman BCMA antibody mixed with serial dilutions of serum samples, and then added to a streptavidin MSD plate. Electricity was applied to the plate electrodes by an MSD instrument leading to light emission by Sulfo-tag labels. Light intensity was then measured to quantify analytes in the sample. The

lowest quantifiable detection value of the assay was defined as 1.0 ng/mL.

Statistical analysis

All statistical analyses were performed in R (v4.2.2), and plots were generated using ggplot2 (v3.5.1). To aid data visualization, some data points may not have been shown on plots (see figure legends); however, all data points were retained in the dataset and included in overall statistical analyses.

Unpaired, 2-sided Wilcoxon rank-sum tests were performed using the wilcox.test function.

Supplemental Tables

Supplemental Table 1. Antibody panel for CyTOF analysis of peripheral blood samples.

Specificity	Clone	Metal isotope	Purpose	Type
CD45	HI30	89Y	Leukocytes	Phenotypic
CD39	Clone A 1	112Cd	B cells, T cells	Phenotypic
CD66b	80H3	113Cd	Granulocytes	Phenotypic
Active caspase 3	C92-605	141Pr	Apoptotic cells	Reference
NKp80	5D12	142Nd	NK-associated activating receptor	Functional
CD3	UCHT1	143Nd	T lymphocytes	Phenotypic
CD11b	ICRF44	144Nd	Monocytes, NK cells	Phenotypic
CD4	RPA-T4	145Nd	T-helper lymphocytes	Phenotypic
CD8	RPA-T8	146Nd	Cytotoxic T lymphocytes	Phenotypic
TIGIT	MBSA43	147Sm	NK and T cells	Functional
CD127	eBioRDR5	148Nd	Activated and regulatory T cells	Phenotypic
CD45RO	UCHL1	149Sm	Memory T lymphocytes	Phenotypic
CD160	688327	150Nd	NK and T cells	Functional
CD33	WM53	151Eu	Myeloid cells	Phenotypic
NKp44	P44-8	152Sm	NK-associated activating receptor	Functional
CD366 (TIM-3)	344823	153Eu	Effector T cells, T cell dysfunction	Functional
CD45RA	HI100	154Sm	Naive T lymphocytes	Phenotypic
CD27	L128	155Gd	Memory B lymphocytes, T lymphocytes	Phenotypic
TOX	REA473	156Gd	T cells, drives T cell exhaustion	Functional
CD137	4B4-1	158Gd	Activated NK cells	Functional

CD123	9F5	159Tb	Plasmacytoid dendritic cells, basophils	Phenotypic
CD69	FN50	160Gd	T cell early activation	Functional
CD28	CD28.2	161Dy	T cell costimulation	Phenotypic
CD11c	Bu15	162Dy	Monocytes, myeloid dendritic cells	Phenotypic
Granzyme B	GB11	163Dy	Activated T cells, NK cells	Phenotypic
NKG2D	1D11	164Dy	NK and T cells	Functional
KLRG1	SA231A2	165Ho	NK and T cells	Functional
GPRC5D	571961	166Er	Plasma cells	Functional
CD19	HIB19	167Er	B lymphocytes	Phenotypic
CD269 (BCMA)	Vicky	168Er	Plasma cells	Functional
CD25	M-A251	169Tm	Activated and regulatory T lymphocytes	Phenotypic
CD279 (PD-1)	EH12-1	170Er	T cell coinhibitory receptor/dysfunction	Functional
CD14	HCD14	171Yb	Monocytes, macrophages	Phenotypic
CD38	HuMax	172Yb	Activation, plasma cells	Functional
CD223 (LAG-3)	17B4	173Yb	T cell coinhibitory receptor	Functional
HLA-DR	646-6	174Yb	Dendritic cells, monocytes, B lymphocytes, T cell activation	Phenotypic
Tbet	4B10	175Lu	T cell associated transcription factor	Functional
CD56	R19-760	176Yb	NK and NKT cells	Phenotypic
DNA	Intercalator	191Ir, 193Ir	Nucleated cells	DNA
CD95	DX2	195Pt	Blast cells	Functional
CD16	3G8	209Bi	Proinflammatory monocytes, NK subset, granulocytes	Phenotypic

BCMA, B-cell maturation antigen; CTLA4, cytotoxic T-lymphocyte–associated protein 4; CyTOF, cytometry by time of flight; GPRC5D, G protein–coupled receptor family C group 5 member D; HLA-DR, human leukocyte antigen DR; Ig, immunoglobulin; LAG-3, lymphocyte activation gene-3; NK, natural killer; NKT, natural killer T cell; PD-1, programmed death-1; PD-L1, programmed death ligand-1; TIM-3, T cell immunoglobulin mucin-3.

Supplemental Table 2. Antibody panel for CyTOF analysis of bone marrow samples.

Specificity	Clone	Metal isotope	Purpose	Type
CD45	HI30	89Y	Leukocytes	Reference
TCRgd	B1	175Lu	γδ T cells	Phenotypic
FOXP3	PCH101	162Dy	Transcription factor	Phenotypic
CD28	CD28.2	142Nd	Costim, development, and survival	Functional
CD3	UCHT1	170Er	T lymphocytes	Phenotypic
CD4	RPA-T4	176Yb	T-helper lymphocytes	Phenotypic
CD8	RPA-T8	146Nd	Cytotoxic T lymphocytes	Phenotypic
Perforin	dG9	152Sm	Cytolytic cytokine	Functional
CD127	eBioRDR5	166Er	Activated and regulatory T cells	Phenotypic
CCR7	150503	172Yb	Activated, memory cells	Phenotypic
CCR4	L291H4	149Sm	Treg effector type	Phenotypic
Nrp1	12C2	151Eu	Treg stability, checkpoint	Functional
BCMA	19F2	156Gd	Plasma cells	Phenotypic
CD366 (TIM-3)	344823	161Dy	Effector T cells, T cell dysfunction	Functional
CD45RA	HI100	153Eu	Naive T lymphocytes	Phenotypic
CD27	L128	155Gd	Memory B lymphocytes, T lymphocytes	Phenotypic
CD152 (CTLA4)	L3D10	160Gd	Regulatory T cells, T cell activation	Functional
CD137	4B4-1	167Er	Activated NK cells	Functional
CD314 (NKG2D)	1D11	158Gd	NK-associated activating receptor	Functional
CD69	FN50	144Nd	T cell early activation	Functional
Granzyme B	GB11	141Pr	Activated T cells, NK cells	Functional
KLRG1	SA231A2	173Yb	Immune checkpoint receptor	Functional
TIGIT	A15153G	116Cd	Checkpoint marker	Functional
CD278 (ICOS)	C398.4A	148Nd	Costim molecule, activated T cells	Functional
CD25	M-A251	169Tm	Activated and regulatory T lymphocytes	Phenotypic
CD279 (PD-1)	EH12-1	145Nd	T cell coinhibitory receptor/dysfunction	Functional
CD161	HP-3G10	168Er	Cytokine-producing Tregs, NK activation receptor	Functional

CD38	HUMAB003	165Ho	Activation, plasma cells	Functional
CD223 (LAG-3)	11C3C65	147Sm	T cell coinhibitory receptor	Functional
HLA-DR	L243	174Yb	Dendritic cells, monocytes, B lymphocytes, T cell activation	Functional
CD57	NK-1	154Sm	Activation marker in NK cells	Phenotypic
CD56	R19-760	163Dy	NK and NKT cells	Phenotypic
DNA	Intercalator	191Ir, 193 Ir	Nucleated cells	DNA
Ki67	Ki-67	164Dy	Proliferating cells	Functional
EOMES	WD1928	143Nd	Transcription factor	Functional
CD16	3G8	209Bi	Monocytes, NK subset, granulocytes	Phenotypic
TCF-1	C63D9	171Yb	Transcription factor	Functional
GPRC5D	GC5B483	159Tb	Plasma cells	Phenotypic
TOX	E6G50	150Nd	Transcription factor	Functional
CD14	M5E2	111Cd	Myeloid lineage	Phenotypic
CD19	HIB19	112Cd	B cells	Phenotypic
CD66b	913542	113Cd	Granulocytes	Phenotypic
CD138	MI15	114Cd	Plasma cells	Phenotypic
CXCR2	5E8-C7-F10	194Pt	Chemokine receptor	Functional
CXCR4	12G5	198Pt	Chemokine receptor	Functional

BCMA, B-cell maturation antigen; CCR4, C-C motif chemokine receptor 4; CCR7, C-C motif chemokine receptor 7; CTLA4, cytotoxic T-lymphocyte–associated protein 4; CXCR2, C-X-C chemokine receptor type 2; CXCR4, C-X-C chemokine receptor type 4; CyTOF, cytometry by time of flight; Eomes, eomesodermin; FOXP3, forkhead box P3; GPRC5D, G protein–coupled receptor family C group 5 member D; HLA-DR, human leukocyte antigen DR; ICOS, inducible T-cell costimulator; KLRG1, killer cell lectin-like receptor G1; LAG-3, lymphocyte activation gene-3; NK, natural killer; NKG2D, natural killer group 2D receptor; NKT, natural killer T cell; Nrp1, neuropilin 1; PD-1, programmed death-1; TCF-1, T cell factor 1; TCRgd, T cell receptor gamma delta; TIGIT, T cell immunoglobulin and ITIM domain; TIM-3, T cell immunoglobulin mucin-3; TOX, thymocyte selection-associated high mobility group box; Treg, immunosuppressive regulatory T cell.

Supplemental Figures

Supplemental Figure 1. Schematic of sample collection.

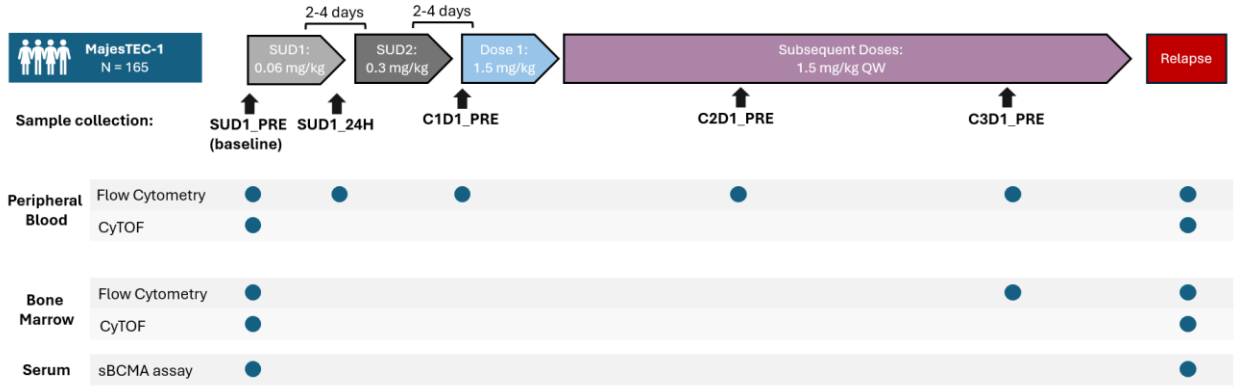

The pivotal recommended phase 2 dose cohort comprised 165 patients who received subcutaneous teclistamab 1.5 mg/kg weekly, following step-up doses (0.06 mg/kg and 0.3 mg/kg). Treatment with teclistamab continued once weekly until disease progression, unacceptable toxicity, withdrawal of consent, or death, whichever occurred first. Patients were allowed to switch to less frequent dosing (once every 2 weeks) if they achieved at least a partial response (≥PR) for a minimum of 4 cycles during phase 1, or a complete response or better for ≥6 months in phase 2. Peripheral blood, bone marrow, and serum samples were collected at step-up dose 1 predose (SUD1_PRE; baseline) and at various longitudinal timepoints for analysis by flow cytometry, CyTOF (cytometry by time of flight), or a soluble B cell maturation antigen (sBCMA) electrochemiluminescence ligand-binding assay using the Meso Scale Discovery (MSD) platform. C, cycle; D, day; QW, every week.

Supplemental Figure 2. Longitudinal expression and maximum fold change of CD38, HLA-DR, and CD25 on CD4+ or CD8+ T cells in the peripheral blood of responders versus nonresponders.

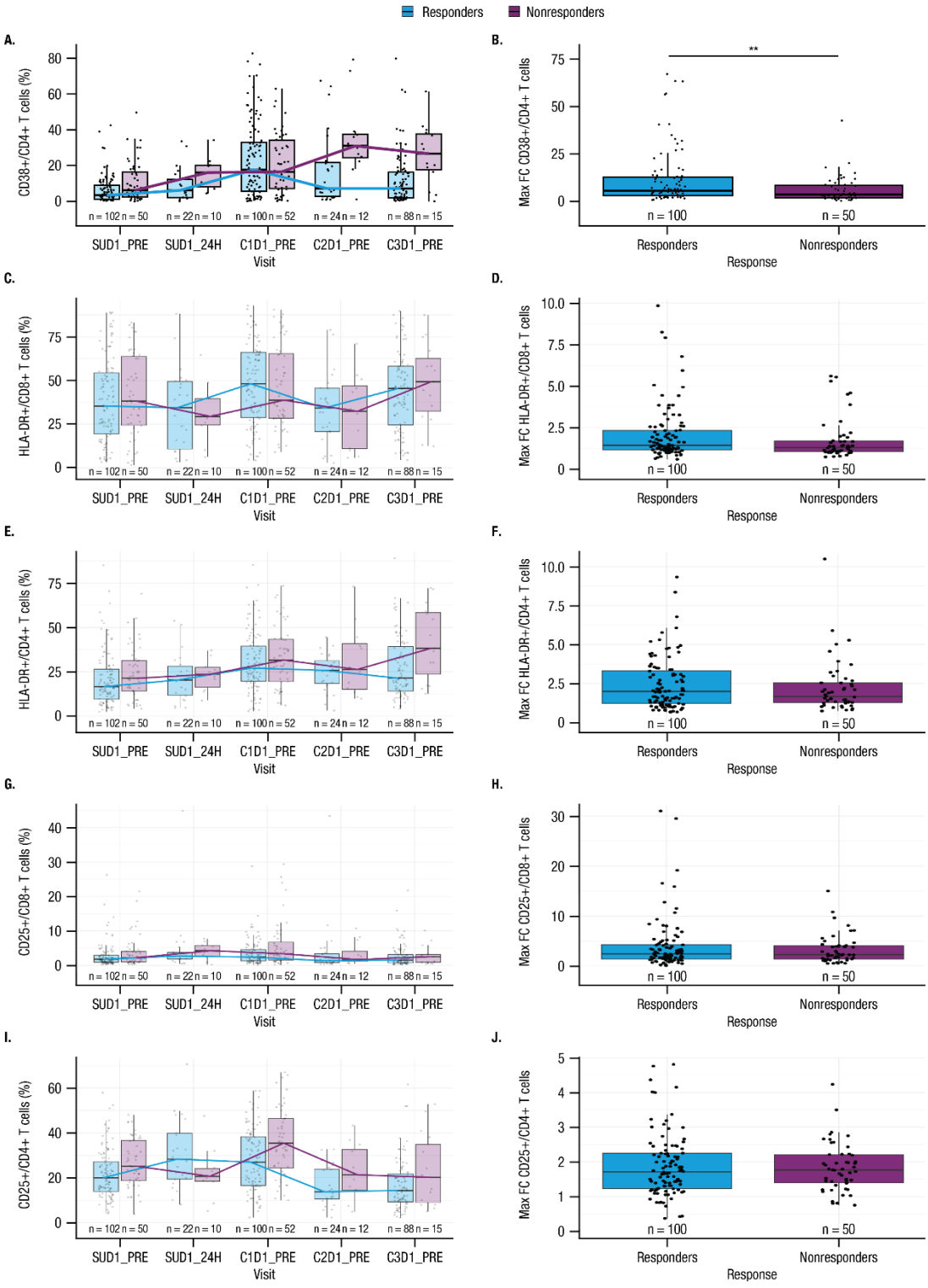

(A) Longitudinal expression of CD38 CD4+ T cells in peripheral blood following administration of first step-up dose (SUD1) of teclistamab. (B) Maximum fold change (max FC) induction of CD38 expression on CD4+ T cells from baseline to C2D1; 2 data points are not shown to improve clarity of the y axis and aid in data visualization (data points were retained in the dataset and included in all statistical analyses). (C) Longitudinal expression of HLA-DR CD8+ T cells in peripheral blood following administration of SUD1 of teclistamab. (D) Max FC induction of HLA-DR expression on CD8+ T cells from baseline to C2D1. (E) Longitudinal expression of HLA-DR CD4+ T cells in peripheral blood following administration of SUD1 of teclistamab. (F) Max FC induction of HLA-DR expression on CD4+ T cells from baseline to C2D1. (G) Longitudinal expression of CD25 CD8+ T cells in peripheral blood following administration of SUD1 of teclistamab. (H) Max FC induction of CD25 expression on CD8+ T cells from baseline to C2D1. (I) Longitudinal expression of CD25 CD4+ T cells in peripheral blood following administration of SUD1 of teclistamab. (J) Max FC induction of CD25 expression on CD4+ T cells from baseline to C2D1. MaxFC was calculated per patient. Data are presented as box plots showing median and interquartile ranges. Statistical significance was assessed using the Wilcoxon rank-sum test, $^{**}P<0.01$. C, Cycle; D, Day; PRE, predose.

Supplemental Figure 3. Longitudinal expression of coinhibitory markers on CD4+ T cells in the peripheral blood of responders versus nonresponders.

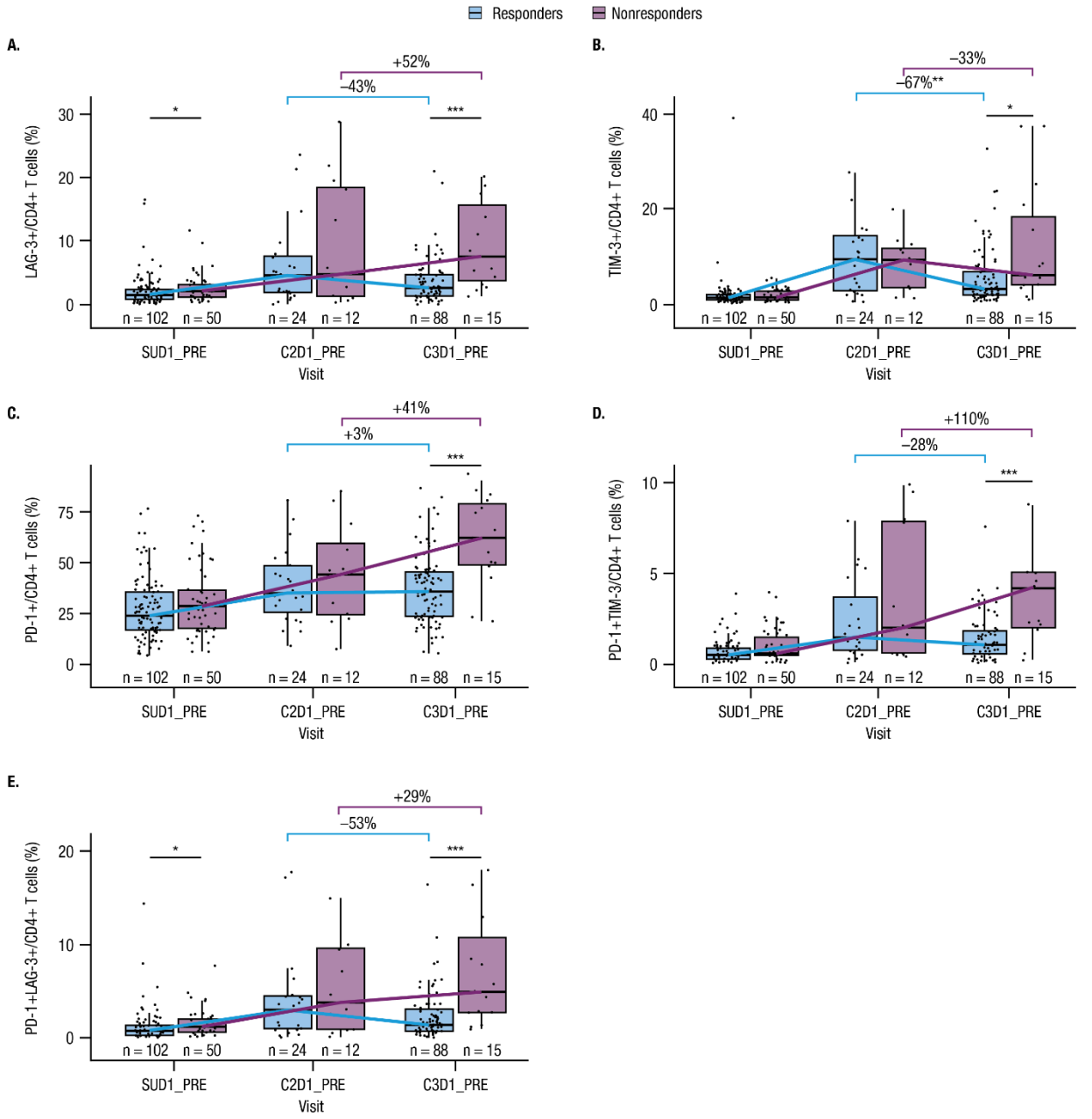

(A) Lymphocyte activation gene-3 (LAG-3) on CD4+ T cells; 4 data points are not shown to improve clarity of the y axis and aid in data visualization (data points were retained in the dataset and included in all statistical analyses).(B) T cell immunoglobulin mucin-3 (TIM-3) on CD4+ T cells; 5 data points are not shown to improve clarity of the y axis and aid in data

visualization (data points were retained in the dataset and included in all statistical analyses). (C) Programmed death-1 (PD-1) on CD4+ T cells. (D) PD-1/TIM-3 on CD4+ T cells; 5 data points are not shown to improve clarity of the y axis and aid in data visualization (data points were retained in the dataset and included in all statistical analyses). (E) PD1-/LAG-3 on CD4+ T cells; 7 data points are not shown to improve clarity of the y axis and aid in data visualization (data points were retained in the dataset and included in all statistical analyses). Data are presented as box plots showing median and interquartile ranges. Statistical significance at SUD1_PRE and C3D1_PRE was assessed using the Wilcoxon rank-sum test, **P*<0.05, ***P*<0.01, ****P*<0.001. C, Cycle; D, Day; PRE, predose; SUD1, step-up dose 1.

Supplemental Figure 4. Changes in expression of checkpoint and inhibitory receptors at relapse on peripheral blood T cells, and regulatory T cells in bone marrow by exploratory supervised analyses using CyTOF.

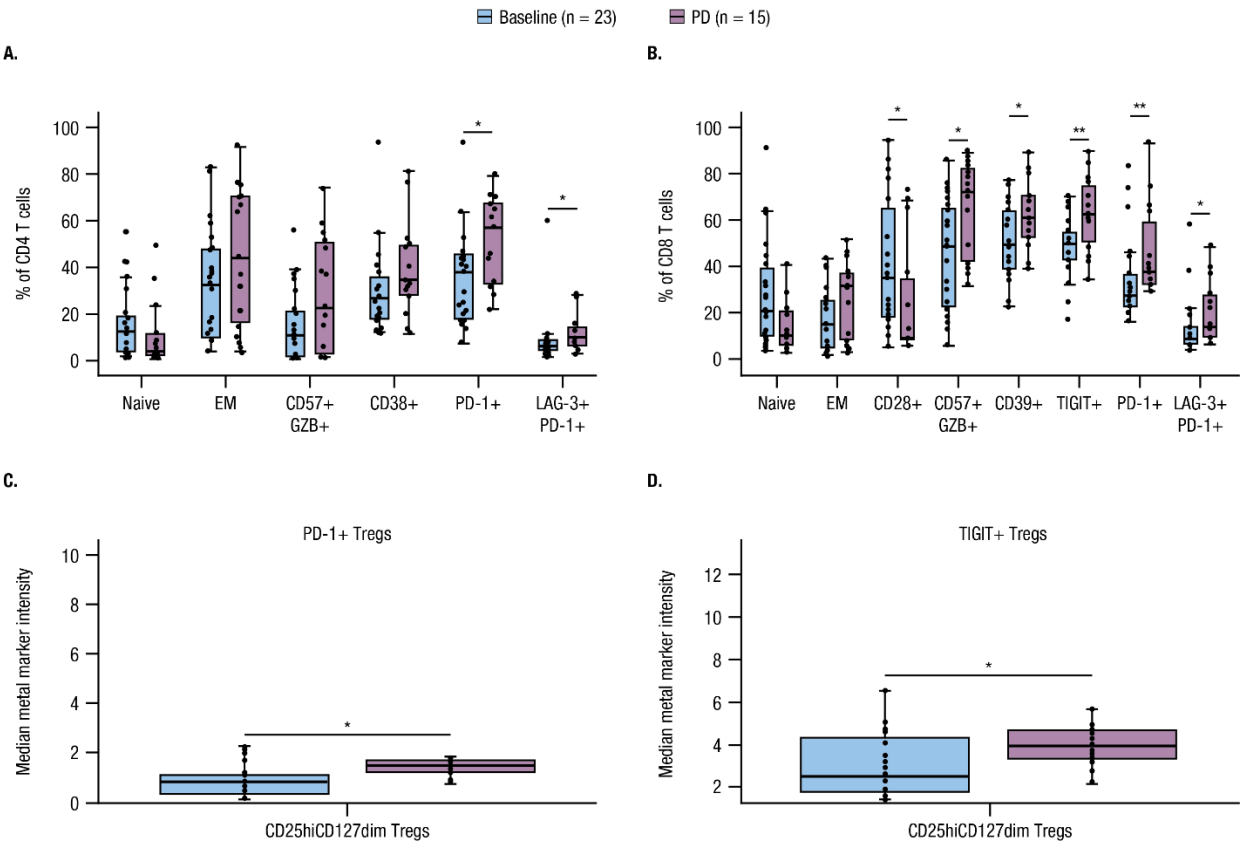

Peripheral blood (PB, A-B) and bone marrow (BM, C-D) samples from patients treated with teclistamab were collected at baseline and at progressive disease (PD) for T cell profiling by CyTOF (cytometry by time of flight). Frequencies of memory and phenotypic T cell subsets were assessed in peripheral CD4 (A) and CD8 (B) T cells at baseline and at disease progression. Median metal marker intensity, representative of relative expression, for programmed death-1 (PD-1; C) and T cell immunoglobulin and immunoreceptor tyrosine-based inhibitory motif domain (TIGIT; D) were evaluated on the bone marrow immunosuppressive regulatory T cells (Tregs; CD3+CD4+CD25hiCD127-/lo), at baseline and PD. Data are presented as box plots showing median and interquartile ranges. Statistical significance was assessed using the

Wilcoxon rank-sum test *P<0.05, **P<0.01. EM, effector memory; GZB, granzyme B; LAG-3, lymphocyte activation gene-3.

Supplemental Figure 5. Proportion of CD8+ and CD4+ T cell counts at the time of disease progression, compared with baseline, in the bone marrow in patients who relapsed.

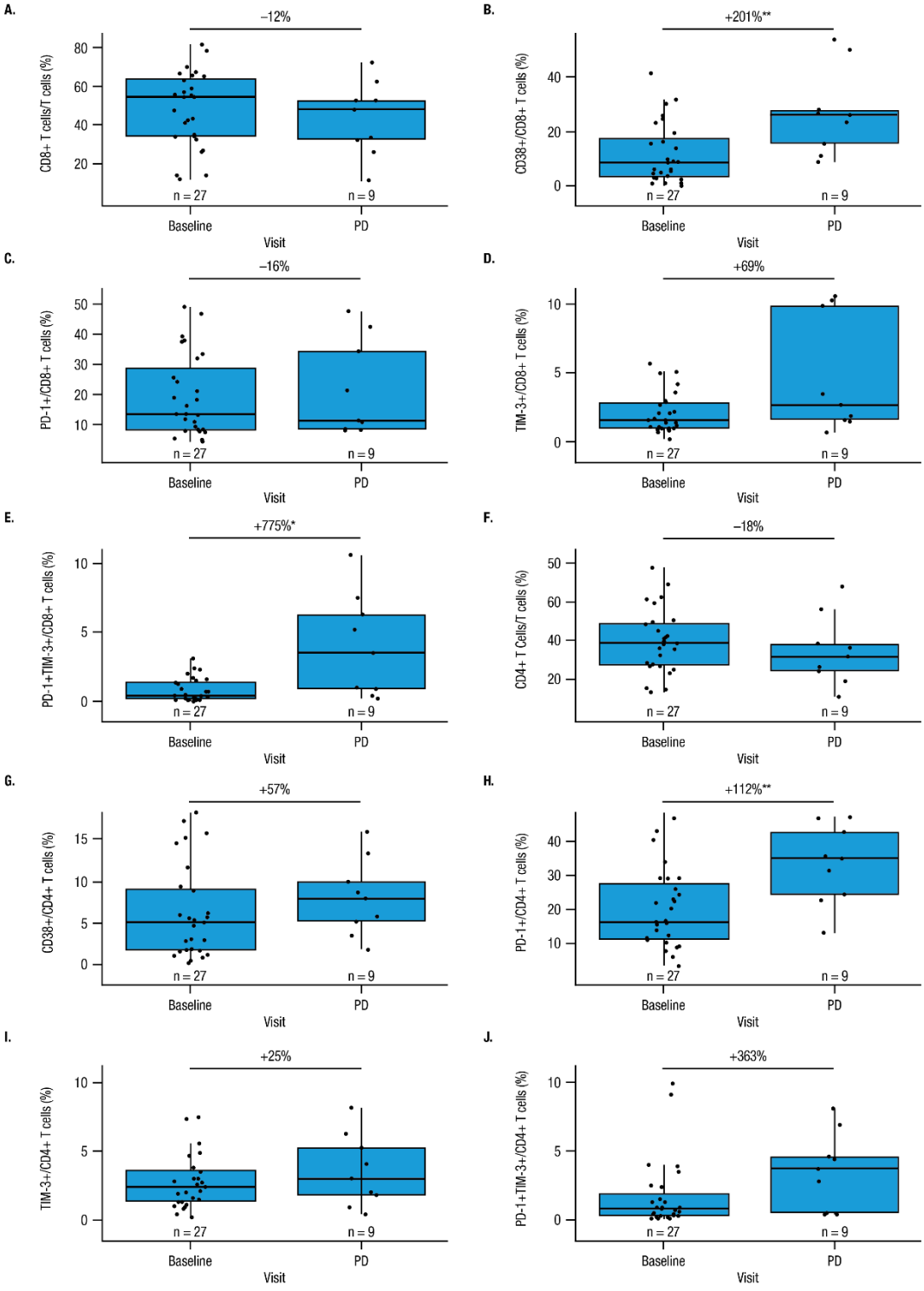

(A) CD8+ T cells. (B) CD38-expressing CD8+ T cells. (C) Programmed death-1 (PD-1) on CD8+ T cells. (D) T cell immunoglobulin mucin-3 (TIM-3) on CD8+ T cells. (E) PD-1/TIM-3 on CD8+ T cells. (F) CD4+ T cells. (G) CD38-expressing CD4+ T cells. (H) PD-1 on CD4+ T cells. (I) TIM-3 on CD4+ T cells; 1 data point is not shown to improve clarity of the y axis and aid in data visualization (data points were retained in the dataset and included in all statistical analyses). (J) PD-1/TIM-3 on CD4+ T cells. Data are presented as box plots showing median and interquartile ranges. Statistical significance was assessed using the Wilcoxon rank-sum test, **P*<0.05, ***P*<0.01. C, Cycle; D, Day; LAG-3, lymphocyte activation gene-3; PD, progressive disease.

Supplemental Figure 6. Proportion of CD8+ and CD4+ T cell counts and CD38+ regulatory T cells at the time of disease progression, compared with baseline, in the peripheral blood in patients who relapsed.

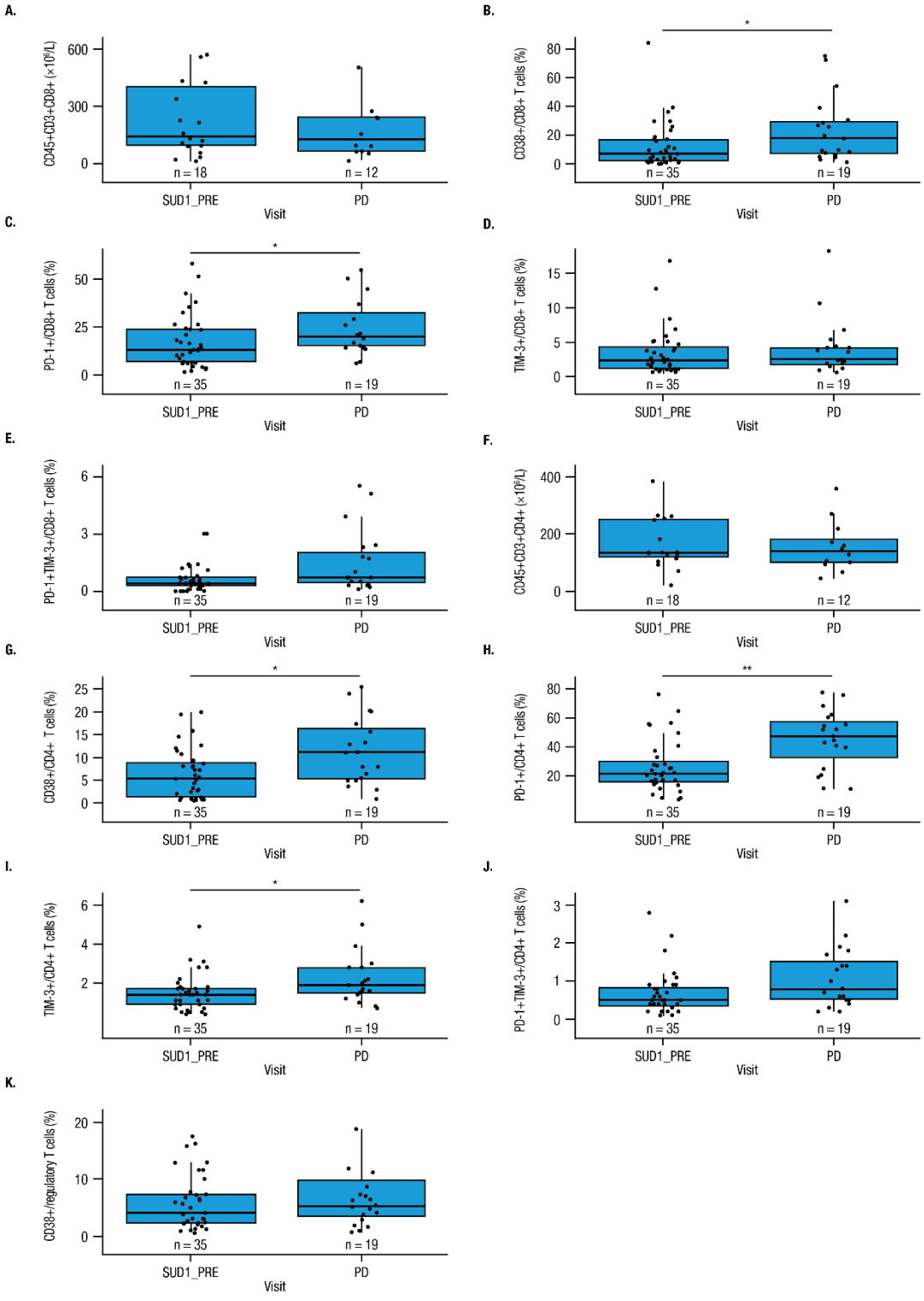

(A) CD8+ T cells; 2 data points are not shown to improve clarity of the y axis and aid in data visualization (data points were retained in the dataset and included in all statistical analyses). (B) CD38-expressing CD8+ T cells. (C) Programmed death-1 (PD-1) on CD8+ T cells; 1 data point is not shown to improve clarity of the y axis and aid in data visualization (data points were retained in the dataset and included in all statistical analyses). (D) T cell immunoglobulin mucin-3 (TIM-3) on CD8+ T cells. (E) PD-1/TIM-3 of CD8+ T cells; 1 data point is not shown to improve clarity of the y axis and aid in data visualization (data points were retained in the dataset and included in all statistical analyses). (F) CD4+ T cells; 1 data point is not shown to improve clarity of the y axis and aid in data visualization (data points were retained in the dataset and included in all statistical analyses). (G) CD38-expressing CD4+ T cells. (H) PD-1 on CD4+ T cells. (I) TIM-3 on CD4+ T cells. (J) PD-1/TIM-3 on CD4+ T cells. (K) CD38-expressing regulatory T cells (Tregs); 2 data points are not shown to improve clarity of the y axis and aid in data visualization (data points were retained in the dataset and included in all statistical analyses). Data are presented as box plots showing median and interquartile ranges. Statistical significance was assessed using the Wilcoxon rank-sum test, *P<0.05, **P<0.01. C, PD, progressive disease; PRE, predose; SUD1, step-up dose 1.

Supplemental Figure 7. Proportion of CD8+ and CD4+ T cell counts and CD38+ regulatory T cells at baseline and the end of treatment in the peripheral blood of responders who relapsed compared to nonresponders.

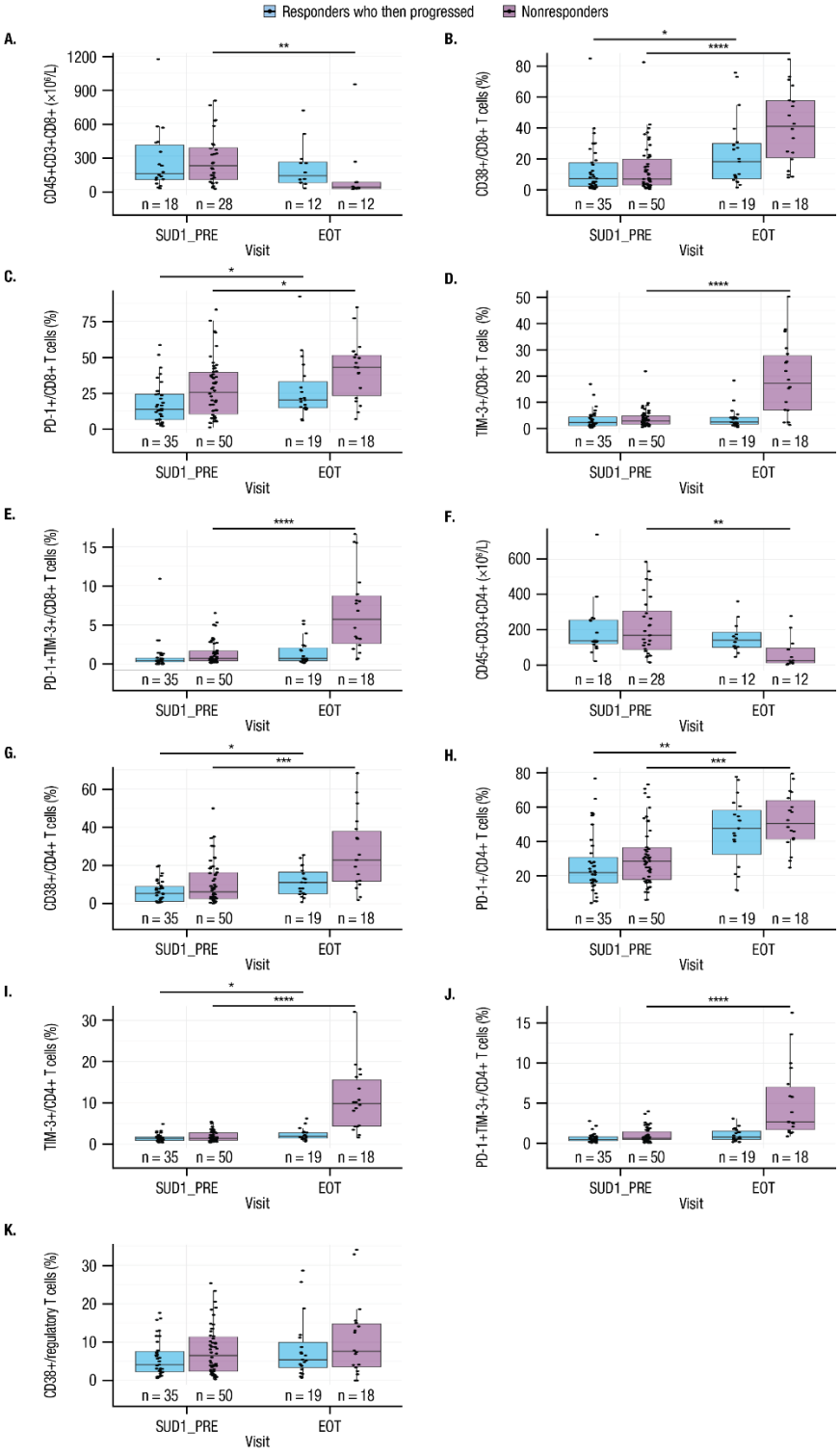

(A) CD8+ T cells. (B) CD38-expressing CD8+ T cells. (C) Programmed death-1 (PD-1) on CD8+ T cells. (D) T cell immunoglobulin mucin-3 (TIM-3) on CD8+ T cells. (E) PD-1/TIM-3 of CD8+ T cells. (F) CD4+ T cells. (G) CD38-expressing CD4+ T cells. (H) PD-1 on CD4+ T cells. (I) TIM-3 on CD4+ T cells. (J) PD-1/TIM-3 on CD4+ T cells. (K) CD38-expressing regulatory T cells (Tregs). Data are presented as box plots showing median and interquartile ranges. Statistical significance was assessed using the Wilcoxon rank-sum test, *P<0.05, **P<0.01, ***P<0.001, ****P<0.0001. EOT, end of treatment; PRE, predose; SUD1, step-up dose 1.

Supplemental Figure 8. Soluble BCMA, proportion of BCMA+ plasma cells, and BCMA receptor density in evaluable patients who relapsed, compared with baseline.

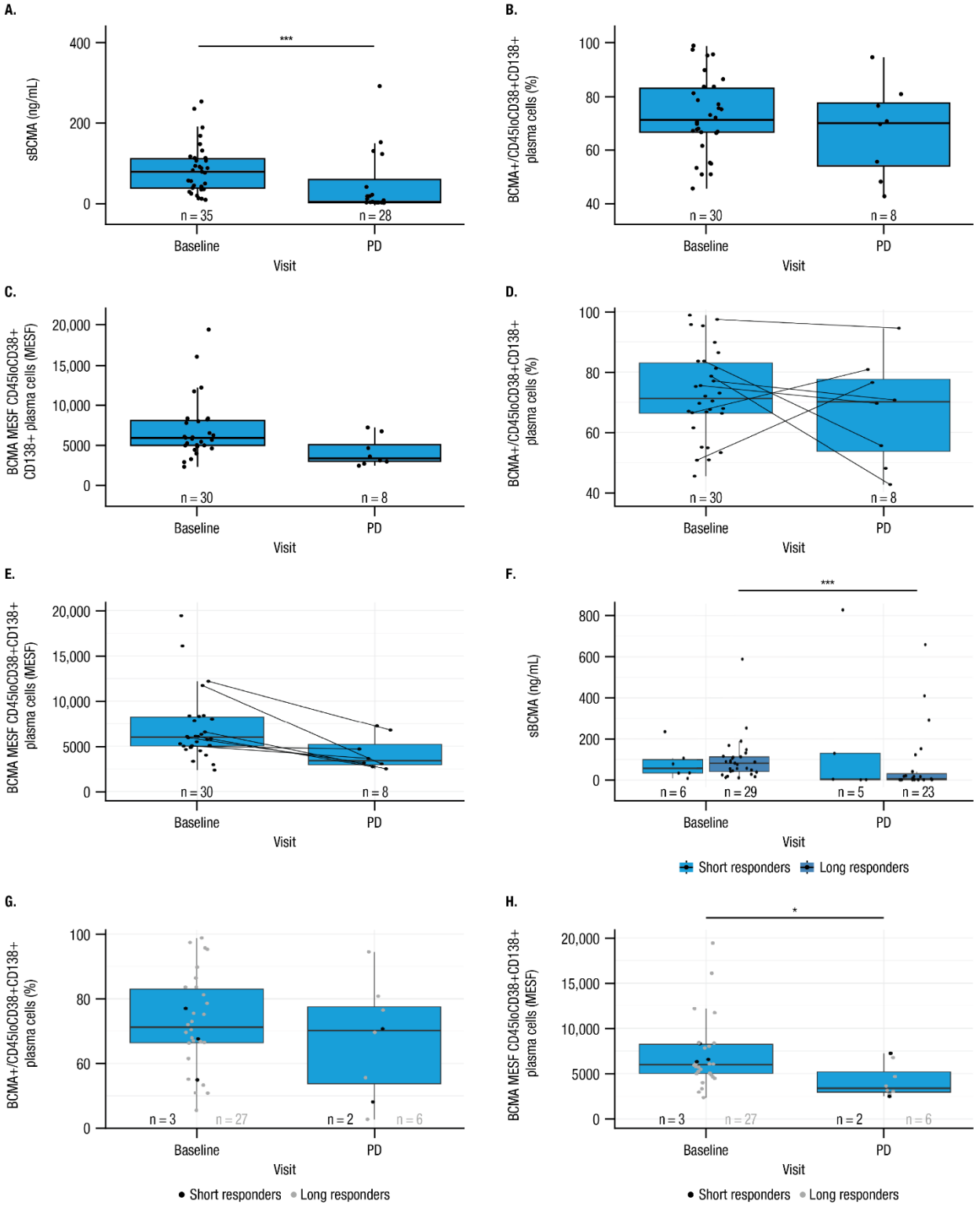

Evaluable patients were those who had available bone marrow samples for analysis. (A) Soluble B cell maturation antigen (sBCMA) levels; 4 data points are not shown to improve clarity of the y axis and aid in data visualization (data points were retained in the dataset and included in all statistical analyses). (B) Proportion of BCMA+ plasma cells out of total number of plasma cells. (C) BCMA receptor density. (D, E) Within-patient paired samples for patients that responded and then progressed for (D) the proportion of BCMA+ plasma cells out of total number of plasma cells [same as panel B with paired samples indicated] and (E) BCMA receptor density [same as panel C with paired samples indicated]. (F) Soluble BCMA levels for short (<6 months) and long (≥6 months) responders. (G) Proportion of BCMA+ plasma cells and (H) BCMA receptor density stratified by short (<6 months) and long (≥6 months) responders [Panels G and H are the same as panels B and C, respectively, with short and long responders indicated]. In panels C, E, and H, 1 data point in the baseline group is not shown (~59,000) to improve clarity of the y axis and aid in data visualization (data points were retained in the dataset and included in all statistical analyses). Data are presented as box plots showing median and interquartile ranges. Statistical significance was assessed using the Wilcoxon rank-sum test, **P*<0.05, ****P*<0.001. MESF, molecules of equivalent soluble fluorochrome; PD, progressive disease; sBCMA, soluble BCMA.

Supplemental Appendix References

1. Moreau P, Garfall AL, van de Donk N, et al. Teclistamab in relapsed or refractory multiple myeloma. N Engl J Med. 2022;387(6):495–505.

2. Usmani SZ, Garfall AL, van de Donk N, et al. Teclistamab, a B-cell maturation antigen × CD3 bispecific antibody, in patients with relapsed or refractory multiple myeloma (MajesTEC-1): a multicentre, open-label, single-arm, phase 1 study. Lancet. 2021;398(10301):665–674.

3. Kumar S, Paiva B, Anderson KC, et al. International Myeloma Working Group consensus criteria for response and minimal residual disease assessment in multiple myeloma. Lancet Oncol. 2016;17(8):e328–e346.

4. Rajkumar SV, Harousseau JL, Durie B, et al. Consensus recommendations for the uniform reporting of clinical trials: report of the International Myeloma Workshop Consensus Panel 1. Blood. 2011;117(18):4691–4695

5. Abraham Y, Neri M. HilbertSimilarity: estimating sample similarity in single cell high dimensional datasets. Version 0.4.3. https://doi.org/10.5281/zenodo.3557362. Accessed 25 April 2022

6. Qiu P. Inferring phenotypic properties from single-cell characteristics. PLoS One. 2012;7(5):e37038.

7. Diggins KE, Greenplate AR, Leelatian N, Wogsland CE, Irish JM. Characterizing cell subsets using marker enrichment modeling. Nat Methods. 2017;14(3):275-278.

8. Pedersen CB, Dam SH, Barnkob MB, et al. cyCombine allows for robust integration of single-cell cytometry datasets within and across technologies. Nat Commun. 2022;13(1):1698.

9. Van Gassen S, Callebaut B, Van Helden MJ, et al. FlowSOM: using self-organizing maps for visualization and interpretation of cytometry data. Cytometry A. 2015;87(7):636-645.

10. Demsar J, Leban G, Zupan B. FreeViz—an intelligent multivariate visualization approach to explorative analysis of biomedical data. J Biomed Inform. 2007;40(6):661-671.

11. Bank of England. The inflation report projections: understanding the fan chart. Quarterly Bulletin 1998 Q1. https://www.bankofengland.co.uk/quarterly-bulletin/1998/q1/the-inflation-report-projections-understanding-the-fan-chart. Accessed 15 May 2025.

12. Qing M, Zhou T, Perova T, et al. Immune profiling of patients with extranodal natural killer/T cell lymphoma treated with daratumumab. Ann Hematol. 2024;103(6):1989-2001.

13. Verkleij CPM, Frerichs KA, Broekmans MEC, et al. NK cell phenotype is associated with response and resistance to daratumumab in relapsed/refractory multiple myeloma. Hemasphere. 2023;7(5):e881.